Molecular Therapy
Nucleic Acids
Original Article

Overexpression of cytosolic long noncoding RNA cytb protects against pressure-overload-induced heart failure via sponging microRNA-103-3p

Xudong Zhang,[1,2] Shuai Yuan,[1,2] Jingbo Liu,[1] Yuyan Tang,[1] Yan Wang,[1] Jiabing Zhan,[1] Jiahui Fan,[1] Xiang Nie,[1] Yanru Zhao,[1] Zheng Wen,[1] Huaping Li,[1] Chen Chen,[1] and Dao Wen Wang[1]

[1]Division of Cardiology, Tongji Hospital, Tongji Medical College and Hubei Key Laboratory of Genetics and Molecular Mechanisms of Cardiologic Disorders, Huazhong University of Science and Technology, 1095# Jiefang Avenue, Wuhan 430030, China

Long noncoding RNAs (lncRNAs) play crucial roles in cardiovascular diseases. To date, only limited studies have reported the role of mitochondria-derived lncRNAs in heart failure (HF). In the current study, recombinant adeno-associated virus 9 was used to manipulate lncRNA cytb (lnccytb) expression *in vivo*. Fluorescence *in situ* hybridization (FISH) assay was used to determine the location of lnccytb, while microRNA (miRNA) sequencing and bioinformatics analyses were applied to identify the downstream targets. The competitive endogenous RNA (ceRNA) function of lnccytb was evaluated by biotin-coupled miRNA pull-down assays and luciferase reporter assays. Results showed that lnccytb expression was decreased in the heart of mice with transverse aortic constriction (TAC), as well as in the heart and plasma of patients with HF. FISH assay and absolute RNA quantification via real-time reverse transcription PCR suggested that the reduction of the lnccytb transcripts mainly occurred in the cytosol. Upregulation of cytosolic lnccytb attenuated cardiac dysfunction in TAC mice. Moreover, overexpression of cytosolic lnccytb in cardiomyocytes alleviated isoprenaline-induced reactive oxidative species (ROS) production and hypertrophy. Mechanistically, lnccytb acted as a ceRNA via sponging miR-103-3p, ultimately mitigating the suppression of PTEN by miR-103-3p. In summary, we demonstrated that the overexpression of cytosolic lnccytb could ameliorate HF.

INTRODUCTION

Heart failure (HF) is a worldwide public health problem with increasing economic expenditure.[1] HF is commonly characterized by fluid retention and dyspnea, which are caused by ventricular dysfunction.[2] Several mechanisms, including dysregulated noncoding RNAs,[3] overloaded mitochondrial calcium levels,[4] perturbations in cardiac metabolism processes, and abnormal mitochondrial autophagy levels,[5] are involved in the onset and progression of HF. Despite reports of several different targets to combat this condition, its outcome has not improved significantly.[6]

In patients with advanced HF, the changes in cardiac substrate metabolism and increments of reactive oxidative species (ROS) are considered to induce contractile dysfunction. These abnormal alterations are closely related to mitochondrial dysfunction. The mitochondrial electron transport chain generates a proton gradient through complexes I–IV and shuttles electrons into complex V to produce ATP.[7] Among these complexes, complex I and complex III are the leading sites of ROS production. However, complex III possesses more important roles in cardiovascular diseases.[8,9] Further, cytochrome *b* (cytb) is the only mitochondrial-DNA-encoded transcript among the 11 subunits of complex III.[10]

In our previous study, we found that microRNA-21 could upregulate mitochondrial cytb (mt-cytb) expression to reduce elevated blood pressure in spontaneous hypertensive rats.[11] In addition, the overexpression of microRNA-92a-2-5p and microRNA-let7b-5p could ameliorate diabetic cardiomyopathy by increasing mt-cytb.[12] These findings indicate that the mitochondrial cytb transcript plays crucial roles in the progression of cardiovascular diseases.

Long noncoding RNAs (lncRNAs) are RNA species that are longer than 200 nt and are usually not translated into proteins.[13] Numerous lncRNAs function as important regulators during cardiac hypertrophy and HF.[3] Myosin-heavy-chain-associated RNA transcript (Mhrt) protected against pathological hypertrophy by blocking brahma-related gene-1-mediated chromatin remodeling.[14] Antihypertrophic interrelated transcript (Ahit) downregulated myocyte enhancer factor 2A by inducing its trimethylation on H3 lysine 27, thereby mitigating transverse aortic constriction (TAC)-induced

Received 13 June 2021; accepted 6 February 2022;
https://doi.org/10.1016/j.omtn.2022.02.002.

[2]These authors contributed equally

Correspondence: Dao Wen Wang, Division of Cardiology, Tongji Hospital, Tongji Medical College and Hubei Key Laboratory of Genetics and Molecular Mechanisms of Cardiologic Disorders, Huazhong University of Science and Technology, 1095# Jiefang Avenue, Wuhan 430030, China.
E-mail: dwwang@tjh.tjmu.edu.cn
Correspondence: Chen Chen, Division of Cardiology, Tongji Hospital, Tongji Medical College and Hubei Key Laboratory of Genetics and Molecular Mechanisms of Cardiologic Disorders, Huazhong University of Science and Technology, 1095# Jiefang Avenue, Wuhan 430030, China.
E-mail: chenchen@tjh.tjmu.edu.cn

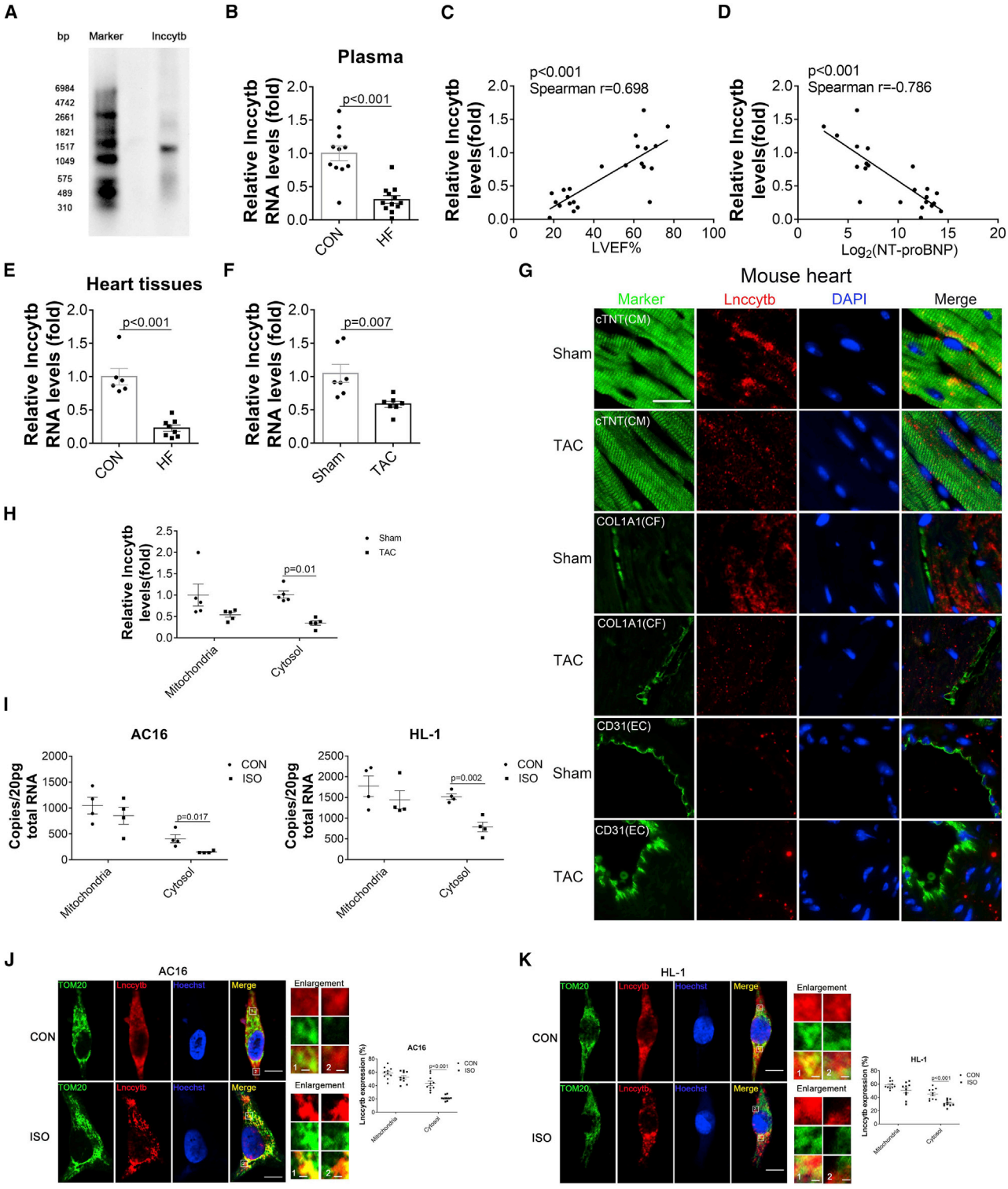

Figure 1. Expressions of lnccytb were decreased in HF patients and mainly reduced in the cytosol of ISO-treated cells and TAC-treated mice

(A) Expression of lnccytb was measured by northern blot in HL-1 mouse cardiac cell. (B) Strand-specific quantitative real-time PCR analysis of lnccytb levels in human plasma, normalization to 18S. CON, n = 11; HF, n = 12. (C) Correlation analysis between lnccytb levels in plasma and LVEF%. (D) Correlation analysis between lnccytb levels in plasma and NT-proBNP. (E) Strand-specific quantitative real-time PCR analysis of lnccytb expressions in the human heart tissues, normalization to 18S. CON, n = 6; HF, n = 8. (F)

(legend continued on next page)

HF.[15] Moreover, lncRNA Plscr4 attenuated hypertrophy by sponging miR-214 and promoted Mitofusin 2 expression.[16]

High-throughput sequencing technology was used to identify a mass of noncoding transcripts in the human mitochondrial transcriptome. Some of these transcripts are located in the opposite strand of protein-coding transcripts, namely lncRNA cytochrome *b* (lnccytb), ND5 (lncND5), and ND6 (lncND6).[17,18] This special location of lnccytb and cytb mRNA reminded us of the phosphatase and tensin homologue (PTEN) and PTEN pseudogene, PTENP1. Moreover, PTENP1 could generate a series of sense and antisense transcripts to regulate PTEN expression at both posttranscriptional and transcriptional levels.[19] Meanwhile, downregulation of PTENP1 expression by CRISPR technology has indicated that PTENP1 could act as a competing endogenous RNA (ceRNA) of PTEN.[20] Hence, whether lnccytb could impact the expression of cytb and the function of mitochondria in HF aroused our great interest.

Several studies have revealed that mitochondria-derived molecules, including mtDNA, tRNA, and lncRNAs, could exist in the cytosol or nucleus and play important roles outside of the mitochondria. Dengue virus infection could promote the translocation of mtDNA to the cytosol and increase the production of interferons by activating the Toll-like receptor 9 signaling pathways.[21] Argonaute 2 (Ago2) was also found to assist in the export of mitochondrial tRNA to the cytosol in 293 cells. Further, the sense mitochondrial ncRNA (SncmtRNA) and two antisense mitochondrial ncRNAs (ASncmtRNAs) were revealed to be exported from the mitochondria to the nucleus in normal and cancer cells.[22] Previously, the plasma mitochondrial lncRNA, LIPCAR, was reported to predict cardiovascular death in patients with HF.[23] Because of the findings of our previous studies, the role of mitochondrial-derived lnccytb in HF garnered our interests.

miRNA-103 (miR-103) belongs to the miR-103/107 family, which is located on chromosome 5 and conservative between human and mouse.[24] miR-103 could promote atherosclerosis and regulate endothelial oxidative injury by inhibiting lncWDR59.[25] Moreover, miR-103/107 increased cardiomyocytes programmed necrosis in myocardial ischemia and reperfusion injury through suppressing Fas-associated protein with death domain.[26] PTEN is an inhibitor of AKT signaling pathway, which was involved in physiological and pathological cardiac hypertrophy.[27–29] Nevertheless, the relationship of miR-103-3p and PTEN in HF remains unexplored.

Accordingly, in the current study, we found that lnccytb was decreased in the cytosol of cardiomyocytes in pressure-overload-induced HF. Further, the underlying mechanism was explored.

RESULTS

lnccytb was mainly reduced in the cytosol *in vitro* and *in vivo*

Although the human lnccytb sequence has been validated by northern blot and rapid amplification of cDNA ends (RACE) technology,[18] its role in HF has not been clarified. Consistently, in mouse mitochondrial transcriptome, there are noncoding regions across the protein-coding cytb strand.[10] Through 5′ and 3′ RACE assays, we identified a 1,149-nt product (Figures S1A–S1C). The full sequence of mouse lnccytb is shown in Table S1. Moreover, alignment of the human lnccytb sequence with mouse lnccytb sequence by Clustal Omega showed up to 71% sequence similarity (Figure S2). Northern blot revealed a product of approximately 1,000 nt in HL-1 mouse cardiac cells (Figure 1A). Based on strand-specific quantitative real-time PCR (ss-quantitative real-time PCR), the plasma level of lnccytb was reduced in HF patients (Figure 1B; Table S5). Moreover, the plasma level of lnccytb was positively correlated with the left ventricular ejection fraction (LVEF) and negatively correlated with the N-terminal pro-brain natriuretic peptide (NT-proBNP) (Figures 1C and 1D). We used Taqman probe and an adaptor RT primer of lnccytb to ensure the PCR products would not possess nuclear pseudogenes; this method was effectively validated by other groups.[18,30] We also performed Sanger sequencing to validate the PCR products that were precisely matched to the mitochondrial genomes instead of the nuclear genomes (Figure S3). A key point is the mechanism that contributes to the decreased expression of lnccytb in the plasma. As exosomes are rich of various ncRNAs, we tested whether lnccytb was able to release into plasma through exosomes. By using exosome inhibitor GW4869 (2 mg/kg), circulating lnccytb RNA level was significantly decreased in animal model, indicating that lnccytb was secreted into plasma by exosome (Figure S4A). Furthermore, the expression level of lnccytb was decreased in the heart tissues of human HF (Figure 1E; Table S6). Meanwhile, as identified by ss-quantitative real-time PCR, lnccytb level in heart tissues was reduced in mice 8 weeks after TAC surgery (Figure 1F). Moreover, fluorescence *in situ* hybridization (FISH) staining of mouse heart sections showed that lnccytb was located in cardiomyocytes (cTNT-positive cells), and the co-localization signal with cardiomyocytes was significantly decreased in TAC-induced HF mice. In contrast, lnccytb signal was barely co-localized with fibroblast- and endothelial-specific markers

Strand-specific quantitative real-time PCR analysis of lnccytb expressions in the mouse heart tissues after TAC operation, normalization to 18S. Sham, n = 7; TAC, n = 7. (G) Co-localization analysis of lnccytb with cardiomyocyte marker cTNT, fibroblast marker COL1A1, and endothelial marker CD31 mouse heart sections by fluorescence *in situ* hybridization (FISH); scale bar, 20 μm. (H) Relative quantitative real-time PCR analysis of lnccytb expressions in the mitochondria and the cytosol of heart tissues after TAC operation (n = 5 per group). (I) Absolute quantitative real-time PCR analysis of lnccytb expressions in the mitochondria and the cytosol in AC16 cells (left) and HL-1 cells (right) after ISO treatment (n = 4 per group). (J) Confocal microscopy showed that co-localization of lnccytb with mitochondria marker TOM20 in AC16 cells by FISH assay (left); scale bars, 10 μm. Boxed areas were enlarged (middle), where the co-localization between lnccytb (red) and TOM20 (green) was shown (n = 10 randomly selected areas); scale bars, 1 μm. Quantification analysis of signaling in 10 randomly selected areas (right) is shown. (K) Confocal microscopy showed co-localization of lnccytb with mitochondria marker TOM20 in HL-1 cells by FISH assay (left); scale bars, 10 μm. Boxed areas were enlarged (middle), where the co-localization between lnccytb (red) and TOM20 (green) was shown (n = 10 randomly selected areas); scale bars, 1 μm. Quantification analysis of signaling in 10 randomly selected areas (right) is shown. (B, E, F, H, and I) Unpaired Student's t test; (C and D) r = Spearman correlation coefficient; (J and K) Mann-Whitney U test. CF, cardiac fibroblast; CM, cardiomyocyte; EC, endothelial cells; LVEF, left-ventricular ejection fraction; NT-proBNP, N-terminal pro-brain natriuretic peptide; data are presented as the mean ± SEM.

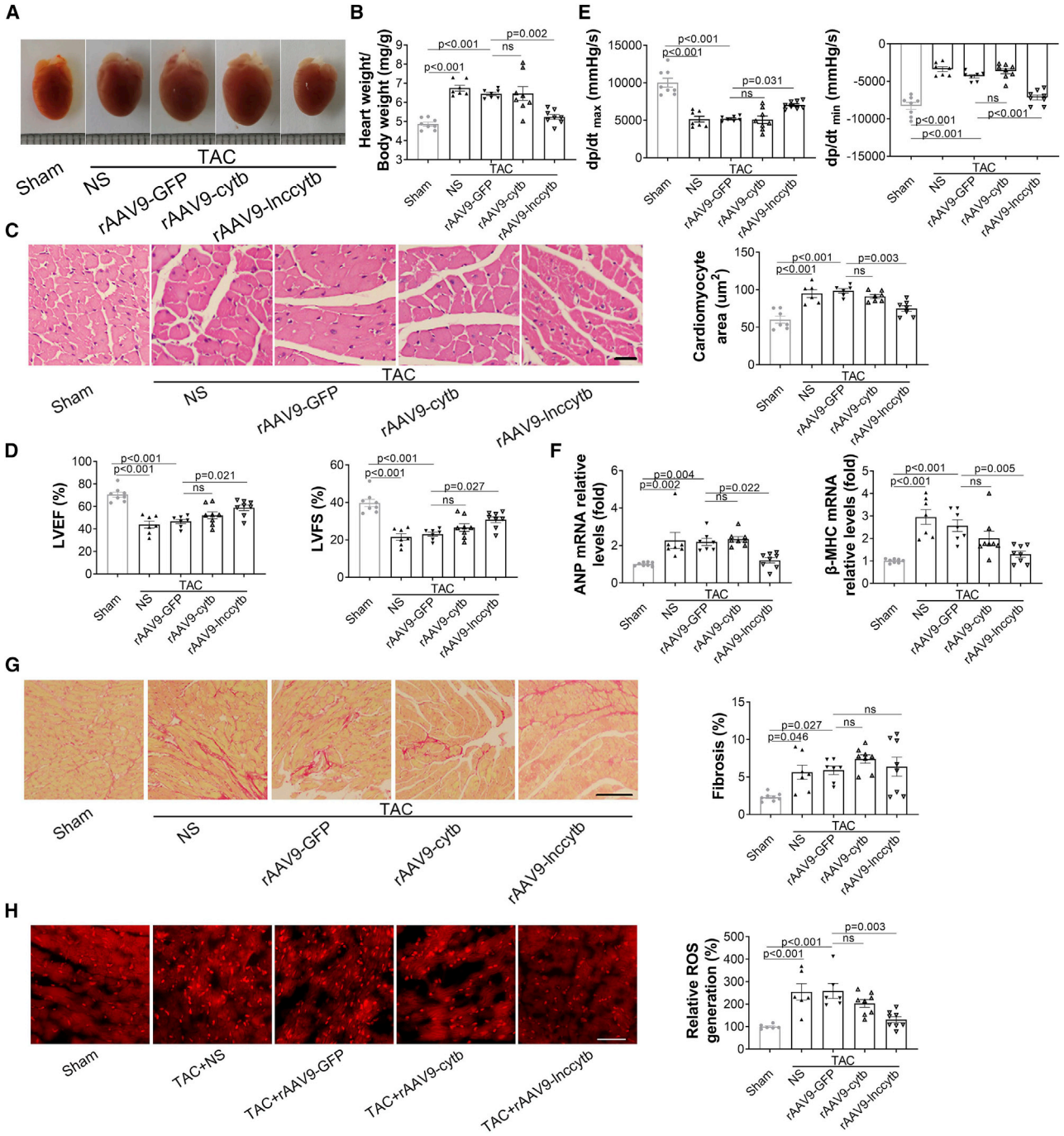

Figure 2. Overexpression of lnccytb in the cytosol could mitigate cardiac function in TAC mice

(A) Representative gross morphologies of hearts in mice with different treatments. (B) The ratios of heart weight to body weight in mice with diverse treatments. (C) Representative images of transverse area of cardiomyocytes detected by H&E (left). Scale bar, 20 μm. The areas of cardiomyocytes were gauged by Image-Pro Plus (right). (D) LVEF% (left) and LVFS% (right) were gauged by echocardiography. (E) Hemodynamic parameters dp/dt_{max} (left) and dp/dt_{min} (right) of mouse hearts were measured by the Millar cardiac catheter system. dp/dt_{max}, peak instantaneous rate of LV pressure increase. dp/dt_{min}, peak instantaneous rate of LV pressure decrease. (F) ANP (left) and β-MHC (right) mRNA expressions in the heart tissues were measured by quantitative real-time PCR from diversely treated mice. (G) Representative images of Sirius Red staining of heart sections from mice with different treatments (left) and quantification analysis of the rate of cardiac fibrosis are shown (right). Scale bar, 100 μm. (H) Representative images of DHE staining of the heart sections from mice with different treatments (left) and quantification analysis of the rate of cardiac ROS generation are

(legend continued on next page)

(Figure 1G). The mitochondria and cytosol from the heart tissues of sham and TAC mice were subsequently extracted. After TAC operation, the reduction of lnccytb mainly occurred in the cytosol instead of the mitochondria, as measured by quantitative real-time PCR (Figure 1H). In order to exclude the impact of nuclear pseudogenes, we extracted the nuclear lysate and employed the absolute quantitative real-time PCR in mitochondria, cytosol, and nucleus, respectively. The results suggested that lnccytb was scarcely located in nucleus and predominantly decreased in cytosol rather than in mitochondria (Figure S4B). The purity of mitochondria and nucleus was shown in Figure S5. *In vitro*, we treated AC16 and HL-1 cell lines by three common cardiac hypertrophy inducers, including angiotensin II (AngII) (1 μM for 24 h), phenylalanine (PE) (50 μM for 24 h), and isoproterenol (ISO) (10 μM for 24 h), while only ISO caused the decrement of lnccytb in both cell lines (Figure S6). In addition, absolute quantitative real-time PCR in AC16 human cardiomyocytes and HL-1 mouse cardiomyocytes suggested that cytosolic lnccytb expression was predominantly decreased after ISO treatment (Figure 1I). FISH assays of AC16 cells and HL-1 cells presented that lnccytb was expressed both in the cytosol and mitochondria under normal conditions. After ISO treatment, the non-co-localization signaling with mitochondria (stained by TOM20) presented significant decrease, indicating that the decrement of lnccytb was mainly in cytosol (Figures 1J and 1K). Moreover, the cytb mRNA and protein levels after TAC operation and in ISO cellular models were reduced (Figure S7).

In summary, the expression level of lnccytb was mainly decreased in the cytosol during the progression of HF.

Overexpression of lnccytb in the cytosol could protect against cardiomyocytes injury *in vivo* and *in vitro*

The reduction of lnccytb expression predominantly occurred in the cytosol; thus, we manipulated lnccytb expression in the cytosol using recombinant adeno-associated virus 9 (rAAV9) vectors (Figure S8). Immunofluorescence staining indicated that rAAV9-GFP exclusively targeted cardiomyocytes in heart tissues (Figure S9). At first, we performed TAC operation after 2 weeks of rAAV injection to explore the potential protective effect of lnccytb. Overexpression of lnccytb ameliorated TAC-induced heart size enlargement as well as the elevated heart weight to body weight (HW/BW) ratio (Figures 2A and 2B). Meanwhile, increased lnccytb expression reduced the area of cardiomyocytes stained by hematoxylin and eosin (H&E) (Figure 2C). Echocardiography indicated that lnccytb overexpression could mitigate the reduction of LVEF and left ventricular fractional shortening (LVFS) caused by TAC operation (Figure 2D). The Millar cardiac catheter system showed consistent results with echocardiography (Figure 2E). In addition, overexpression of the lncRNA prevented the induction of the hypertrophic markers by TAC (Figure 2F). However, the fibrosis induced by TAC operation was not affected by lnccytb overexpression (Figure 2G). Nonetheless, cardiac ROS generation induced by TAC was reduced in lnccytb-treated mice (Figure 2H). Compared with the AAV9-GFP TAC group, overexpression of the across-strand cytb mRNA had no statistically significant effects on all phenotypes. Subsequently, we were supposed to figure out where lnccytb have the therapeutic effects on HF. Thereafter, we injected the same titer of rAAV after 2-week TAC treatment. The results showed that overexpression of cytosolic lnccytb could still protect against the cardiac dysfunction (Figure S10).

In addition, mRNA sequencing was used to determine the downstream pathways of cytosolic lnccytb in mouse HL-1 cardiac cells. The increments in lnccytb expression in the cytosol could upregulate genes that were mainly enriched in the oxidative phosphorylation pathway by Kyoto Encyclopedia of Genes and Genomes (KEGG) analysis (Figure S11A). The efficiency of lnccytb expression and the purity of mitochondria isolation are shown in Figure S12. As the expression level of lnccytb was decreased in the plasma and heart of HF patients, we performed *in vitro* experiments using human cardiac AC16 cells. First, the overexpression of lnccytb could attenuate the ISO-induced ANP and β-MHC mRNA levels in AC16 cells (Figure S11B). Further, the expression of the ANP protein aligned with the mRNA level (Figure S11C). The morphology of cardiac cells stained with fluorescein isothiocyanate (FITC)-phalloidin indicated that upregulated lnccytb could inhibit ISO-induced hypertrophy (Figure S11D). We detected the production of ROS using a dihydroethidium (DHE) probe, which suggested that the overexpression of lnccytb could reduce ISO-induced ROS production (Figure S11E). Meanwhile, mitochondria localized ROS (mtROS) was also lessened by using MitoSOX-RED probe (Figure S11F). In the normal condition without stress, overexpression of lnccytb did not affect these phenotypes (Figures S11G–S11I). In addition, enhanced lnccytb could improve the mitochondrial membrane potential, neither affecting the ATP production nor regulating the expression of mitochondrial-gene-encoded subunits (Figure S13).

In summary, the overexpression of lnccytb in the cytosol could ameliorate cardiomyocytes injury *in vivo* and *in vitro*.

Knockdown of lnccytb could aggravate cardiomyocytes insult *in vivo* and *in vitro*

Knockdown of lnccytb aggravated TAC-induced heart size enlargement as well as the elevated HW/BW ratio (Figures 3A, 3B, and S14A). Meanwhile, reduced lnccytb expression increased the area of cardiomyocytes stained by H&E (Figure 3C). Echocardiography indicated that lnccytb reduction could exacerbate the reduction of LVEF and LVFS caused by TAC operation (Figure 3D). The Millar cardiac catheter system showed consistent results with echocardiography (Figure 3E). In addition, loss of the lncRNA enhanced the induction of the hypertrophic markers by TAC (Figure 3F). However, the fibrosis induced by TAC operation was not affected by lnccytb decline

shown (right). Scale bar, 100 μm. (B–H) Comparisons of parameters were performed with one-way ANOVA followed by Tukey's test for multiple comparisons. DHE, dihydroethidium; H&E, hematoxylin and eosin; LVEF, left ventricular ejection fraction; LVFS, left ventricular fractional shortening; ns, not significant. Sham (n = 8), TAC + NS (n = 7), TAC + rAAV9-GFP (n = 7), TAC + rAAV9-cytb (n = 8), and TAC + rAAV9-lnccytb (n = 8). Data are presented as the mean ± SEM.

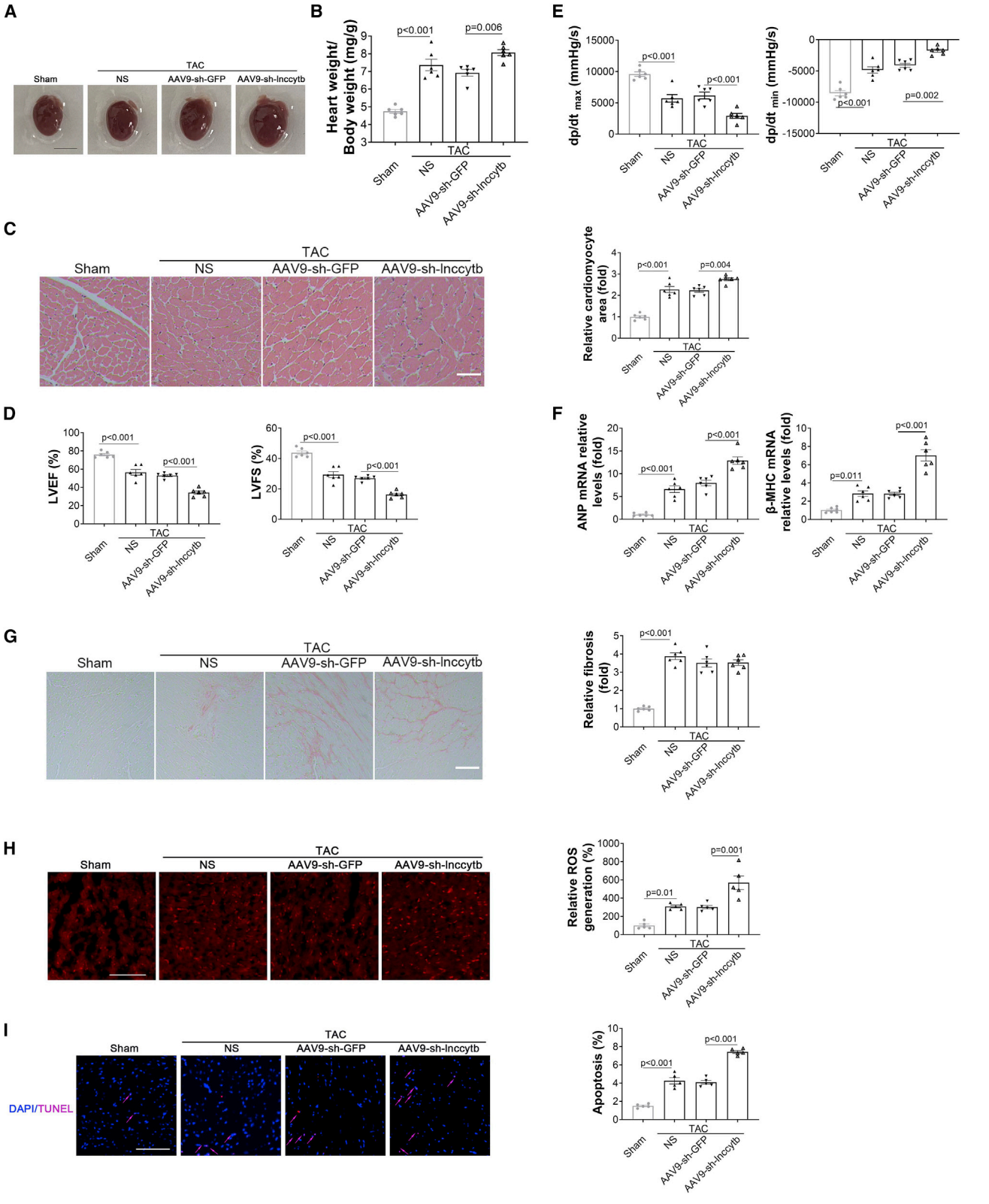

(legend on next page)

(Figure 3G). Nonetheless, cardiac ROS and apoptosis generation induced by TAC were increased in lnccytb knockdown mice (Figures 3H and 3I).

In addition, we reduced lnccytb expression by antisense oligonucleotides (ASOs) *in vitro*. Our data showed that inhibition of lnccytb enhanced cardiomyocytes hypertrophy and ROS generation by ISO treatment (Figure S15). Moreover, this lncRNA did not affect cardiac function in a non-operated control group receiving the AAV9 vector (Figure S16).

In brief, reduction of lnccytb exacerbated cardiomyocytes insult *in vivo* and *in vitro*.

Cytosolic lnccytb could reduce hypertrophy by sponging miR-103-3p

Recently, numerous findings have revealed that cytosolic lncRNAs could participate in the progression of cardiovascular diseases as ceRNAs.[31,32] Hence, we speculated that cytosolic lnccytb might sponge certain miRNAs to affect the functions of cardiomyocytes. Some studies have indicated that miRNAs are more likely inversely correlated networks of ceRNA interaction.[33,34] The candidate miRNAs would be upregulated in TAC-treated mice. Thereafter, we re-analyzed the GSE112054 dataset, which contained the miRNA expression sequencing data for the hearts retrieved from five sham and five TAC mice. A total of 106 miRNAs were significantly increased after TAC operation (Table S2). In addition, the abundance of miRNAs also affected the regulatory capacity and should approach the abundance of the ceRNA.[35] We performed miRNA sequencing using the heart tissues of the three control C57/BL6 mice and listed the transcripts per million (TPM) $\geq$ 50 (Table S3). Sixteen miRNAs were eligible for the selected 106 miRNAs. Meanwhile, considering that user-defined parameters could maximize true positives and minimize false negatives and positives, bioinformatic algorithms were widely used to predict the targeted miRNAs.[36,37] Hence, RegRNA 2.0 (http://regrna2.mbc.nctu.edu.tw/) was then employed to predict the miRNAs targeting lnccytb; this yielded 16 miRNAs by reaching a score $\geq$150 and a free energy ≤ -20 kcal/mol (Table S4). Finally, miR-103-3p was selected as the miRNA most likely to target lnccytb (Figure 4A). The increased expression of miR-103-3p in 8-week-old TAC mice was validated by quantitative real-time PCR (Figure 4B). *In vitro* RNA pull-down assay of mouse heart tissue lysate demonstrated that lnccytb could bind to the Ago2 protein, which also suggested an interaction between lnccytb and miRNAs (Figure 4C). In addition, a biotin-labeled miRNA pull-down assay demonstrated that biotin-labeled miR-103-3p could increase lnccytb enrichment compared with the mimic random (MR) (Figure 4D). Moreover, overexpression of lnccytb could reduce ISO-induced increase of miR-103-3p in AC16 and HL-1 cells (Figure 4E). However, overexpression of miR-103-3p could not decrease ISO-induced reduction of lnccytb in AC16 and HL-1 cells (Figure 4F). Meanwhile, we isolated primary neonatal mouse cardiomyocytes (NMCMs) followed by immunofluorescence verification showing no contamination of cardiac fibroblast, cardiac endothelial cells, and smooth muscle cells (Figure S17A). Using these purified NMCMs, we performed several key studies and found that overexpression of lnccytb could reduce ISO-induced increase of miR-103-3p in NMCMs (Figure S17B). Conversely, overexpression of miR-103-3p could not decrease ISO-induced reduction of lnccytb in NMCMs (Figure S17C). In addition, biotin-labeled miR-103-3p could elevate lnccytb enrichment compared with the MR group in NMCMs (Figure S17D). Absolute quantitation of lnccytb and miR-103-3p showed that there were ~3,300–3,800 lnccytb molecules per cell versus ~4,200–7,100 molecules of miR-103-3p in AC16 cells while ~5,200–7,600 lnccytb molecules per cell versus ~8,000–19,000 molecules of miR-103-3p in HL-1 cells (Figure 4G). Moreover, double FISH of miR-103-3p and lnccytb revealed the co-localization of these two molecules in control human and mouse heart tissues. In addition, co-localization was decreased in HF tissues (Figure 4H). There were two complementary seed regions binding sites of miR-103-3p and lnccytb in both human and mouse sequences, of which binding site one was conserved considering the wobble pairing (Figure 4I). Luciferase reporter gene assays indicated that the relative luciferase activity of pMIR-GLO-lnccytb was significantly suppressed in human HEK293T cells after co-transfection with miR-103-3p mimics. However, this inhibitory effect of miR-103-3p was blocked by mutating binding site one rather than binding site two of lnccytb (Figure 4J). RNA immunoprecipitation (RIP) assays were also carried out to pull down endogenous miR-103-3p associated with lnccytb. Based on the results, lnccytb was significantly enriched by miR-103-3p compared with the empty vector (MS2) in HL-1 cells. By mutating binding site one in lnccytb of mouse, miR-103-3p enrichment was restored to the control level. However, the level of control miR-195a-3p was unchanged (Figure 4K). In addition, co-transfecting miR-103-3p with

Figure 3. Knockdown of lnccytb could aggravate cardiomyocytes insult *in vivo*

(A) Representative gross morphologies of the hearts in mice with different treatments. Scale bar, 5 mm. (B) The ratios of heart weight to body weight in mice with diverse treatments. (C) Representative images of transverse area of cardiomyocytes detected by H&E (left). Scale bar, 10 μm. The areas of cardiomyocytes were gauged by Image-Pro Plus (right). (D) LVEF% (left) and LVFS% (right) were gauged by echocardiography. (E) Hemodynamic parameters dp/dt_{max} (left) and dp/dt_{min} (right) of mouse hearts were measured by the Millar cardiac catheter system. (F) ANP (left) and β-MHC (right) mRNA expressions in the heart tissues were measured by quantitative real-time PCR from diversely treated mice. (G) Representative images of Sirius Red staining of the heart sections from mice with different treatments (left) and quantification analysis of the rate of cardiac fibrosis are shown (right). Scale bar, 10 μm. (H) Representative images of DHE staining of the heart sections from mice with different treatments (left) and quantification analysis of the rate of cardiac ROS generation are shown (right). Scale bar, 30 μm. (I) Representative images of TUNEL staining of heart sections from mice with different treatments (left) and quantification analysis of the rate of cardiac apoptosis are shown (right). TUNEL (red) and DAPI (bule) were shown; scale bar, 30 μm. (B–I) Comparisons of parameters were performed with one-way ANOVA followed by Tukey's test for multiple comparisons. Sham (n = 6), TAC + NS (n = 6), TAC + AAV9-sh-GFP (n = 6), and TAC + AAV9-sh-lnccytb (n = 6). Data are presented as the mean ± SEM.

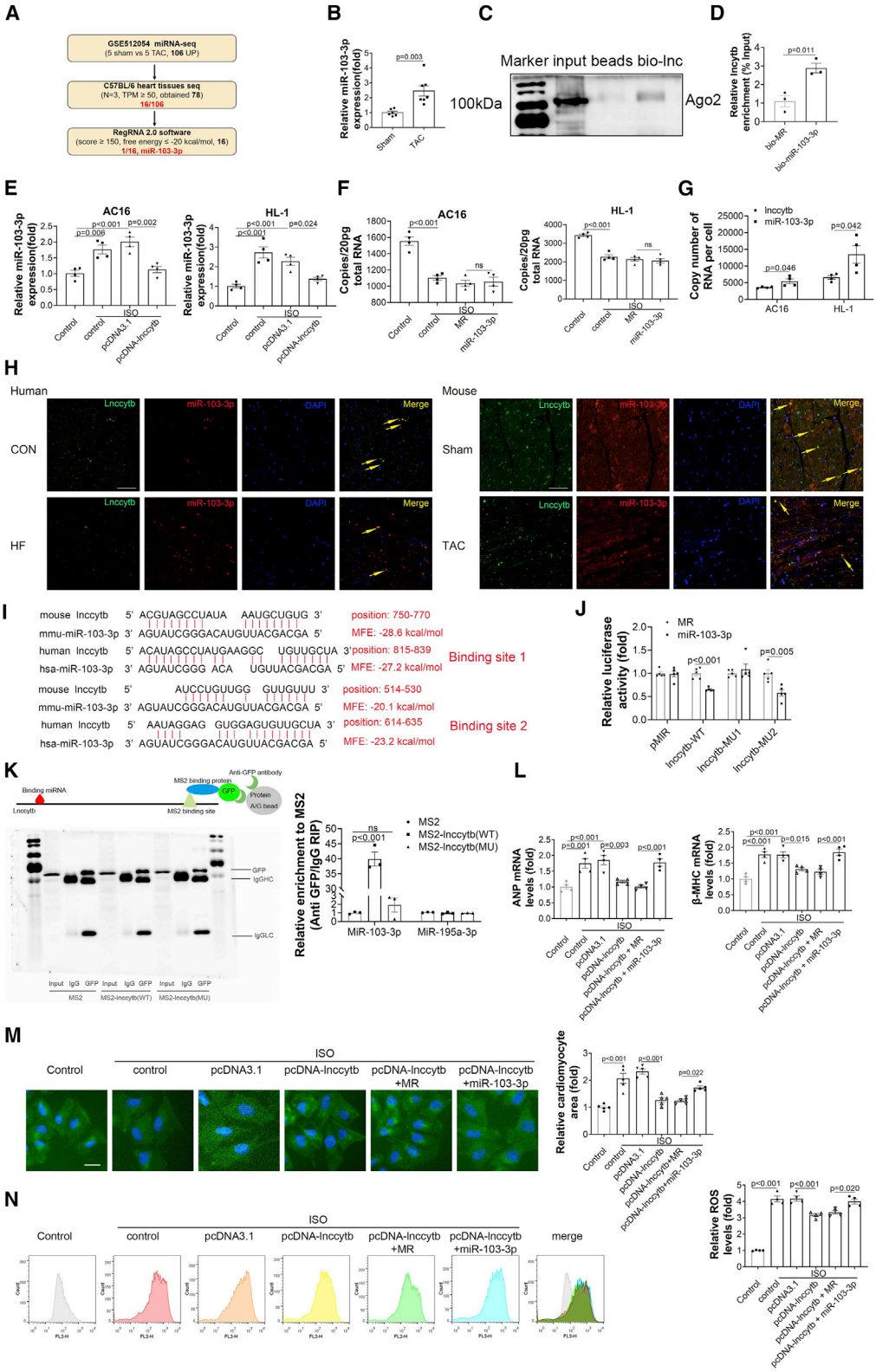

(legend on next page)

pcDNA-lnccytb could attenuate the protective effects of lnccytb on the increased ANP and β-MHC mRNA levels (Figure 4L), cardiomyocyte area (Figure 4M), and ROS generation induced by ISO (Figure 4N). In addition, we constructed the pcDNA-lnccytb-MU1 with the mutated binding site one. And overexpression of the mutated vector could not produce the protective effect in hypertrophy and ROS generation (Figure S18).

RNA pull-down assay is the classical method to study the binding proteins of tagging RNA.[38,39] Moreover, the antisense probe of targeted RNA also decreased the false positives.[40,41] We therefore performed lnccytb pull-down assay in the mitochondria and the cytosol of mouse heart tissues. The adjacent proteins captured by lnccytb and cytb mRNA were subjected to liquid chromatography-mass spectrometry (LC-MS). Because in HF, cytosol cytb mRNA did not show any detectable changes while cytosol lnccytb was decreased, we reasoned that the transporter protein should be closely connected to lnccytb rather than cytb mRNA. As a result, a total of 79 proteins in the mitochondria and 58 proteins in the cytosol were identified to be closely connected with lnccytb, but not cytb, mRNA (Data S1). Among these proteins, G-rich sequence factor 1 (GRSF1), heterogeneous nuclear ribonucleoprotein M (HNRNPM), and 26S proteasome regulatory subunit 6A (PSMC3) were captured by both mitochondrial- and cytosol-localized lnccytb. Then, GRSF1 was selected for further validation because it showed higher abundance in the mitochondria among the three candidates. Indeed, RNA pull-down followed by GRSF1 western blot confirmed that GRSF1 could be pulled down by lnccytb, but not cytb, mRNA both in the mitochondria and cytosol (Figure S19A). More importantly, subsequent functional analysis showed that GRSF1 knockdown indeed decreased the level of lnccytb in the cytosol (Figures S19B and S19C). Interestingly, we observed that GRSF1 was also decreased in HF, which might explain the reduction of lnccytb in the cytosol under disease conditions (Figure S19D).

Aside from the translocation efficiency from the mitochondria into the cytoplasm, we also measured the mitochondrial copy numbers and lnccytb degradation rate in HF. Interestingly, our data suggested that the mitochondrial copy numbers were not changed in TAC-induced cardiac tissues and stressed HL-1 cells (Figures S20A and S20B). Next, we determined to investigate lncRNA lnccytb degradation rate by treating HL-1 cells with mitochondrial transcription inhibitors (actinomycin D). We noticed that ISO intervention did not affect the degradation of lnccytb (Figure S21A). In this case, we first attempted to identify GRSF1, which was responsible for the exporting of lnccytb from the mitochondria into the cytoplasm.

Collectively, these findings indicate that lnccytb in the cytosol could target miR-103-3p and protect against hypertrophy *in vitro*.

miR-103-3p could target PTEN to promote hypertrophy

To investigate the downstream targets of miR-103-3p, we proceeded to screen the following strategies: (1) the top 100 Targetscan bioinformatics prediction websites, (2) the top 100 miRanda bioinformatics prediction websites, and (3) the conservations between human and mouse (Figure 4A). Further, we re-analyzed the GSE112055 dataset, which contained mRNA expression sequencing data of the hearts retrieved from sham and TAC mice. We focused on the counts >100 mRNA data, which yielded eight putative targets. RIP assay with bio-labeled miR-103-3p was performed to detect the putative targets of miR-103-3p. The results showed that miR-103-3p transfection significantly increased the binding mRNA levels of PTEN (Figure 5B). However, overexpression of miR-103-3p decreased the protein levels of PTEN in HL-1 mouse cardiac cells, AC16 human cardiac cells, and NMCMs (Figures 5C–5E). Luciferase assays revealed that the relative luciferase activity of pMIR-GLO-PTEN was significantly inhibited in human HEK293T cells after co-transfection with miR-103-3p. However, the suppressive effects of miR-103-3p were blocked by mutating the binding site in PTEN 3′ UTR (Figure 5F). Co-transfecting miR-103-3p and the PTEN overexpression vector could attenuate the miR-103-3p-induced hypertrophy marker expression and cell area enlargement in ISO-treated cardiomyocytes (Figures 5G and 5H), as well as ROS generation (Figure 5I).

Therefore, miR-103-3p could target PTEN to promote ISO-induced hypertrophy ROS generation *in vitro*.

Figure 4. lnccytb could reduce hypertrophy and ROS production by sponging miR-103-3p

(A) The strategy to identify the putative miRNAs targeted by lnccytb in HF. (B) Expression of miR-103-3p in sham and TAC mice, measured by quantitative real-time PCR. Sham, n = 7; TAC, n = 7. (C) RNA pull-down assay was conducted by incubating biotinylated 3′ end of lnccytb with whole-cell lysate from sham mouse heart tissues. The RNA-protein complex was subjected to western blot. (D) RNA pull-down assays performed in HL-1 cardiomyocytes treated with the biotinylated miR-103-3p mimic (n = 3). (E) Expression of miR-103-3p was detected by quantitative real-time PCR in AC16 cells (left) and HL-1 cells (right) after various treatments (n = 4). (F) Absolute quantitative real-time PCR analysis of lnccytb was performed in AC16 cells (left) and HL-1 cells (right) after overexpression of miR-103-3p (n = 4). (G) Absolute quantitative real-time PCR analysis of lnccytb and miR-103-3p expressions in AC16 and HL-1 cells (n = 4). (H) Co-localization of lnccytb and miR-103-3p in the human heart sections of control and HF (left) was detected by double FISH; co-localization of lnccytb and miR-103-3p in the heart sections from mice with different treatments (right) was detected by double FISH. Scale bars, 50 μm. (I) The binding sites of miR-103-3p and lnccytb between human and mouse. (J) Regulation of lnccytb by miR-103-3p targeting its sequence was detected with luciferase reporter assays in HEK293T cells (n = 5). (K) MS2-RIP followed by miR-103-3p quantitative real-time PCR to detect miR-103-3p endogenously associated with lnccytb in HL-1 cells. Western blot by anti-GFP antibody (left) is shown. miR-103-3p and miR-195a-3p expressions detection by quantitative real-time PCR (right; n = 3) are shown. IgG, immunoglobulin G. (L) Expression of ANP and β-MHC mRNA in AC16 cardiomyocytes with different disposal measured by real-time PCR (n = 4). (M) Representative images of cardiomyocyte areas stained by phalloidin (green) and Hoechst (blue) (left). Scale bar, 20 μm. Quantitative analysis of cell sizes by Image-Pro Plus (right) is shown. (N) ROS levels were stained by DHE probe in AC16 cells with different treatments detected by flow cytometry (n = 4; left); quantitative analysis of flow cytometry data (right). (B, D, G, and J) Student's t test; (E, F, and K–N) one-way ANOVA followed by the Tukey's post hoc analysis was used. MR, mimic random. Data are expressed as mean ± SEM.

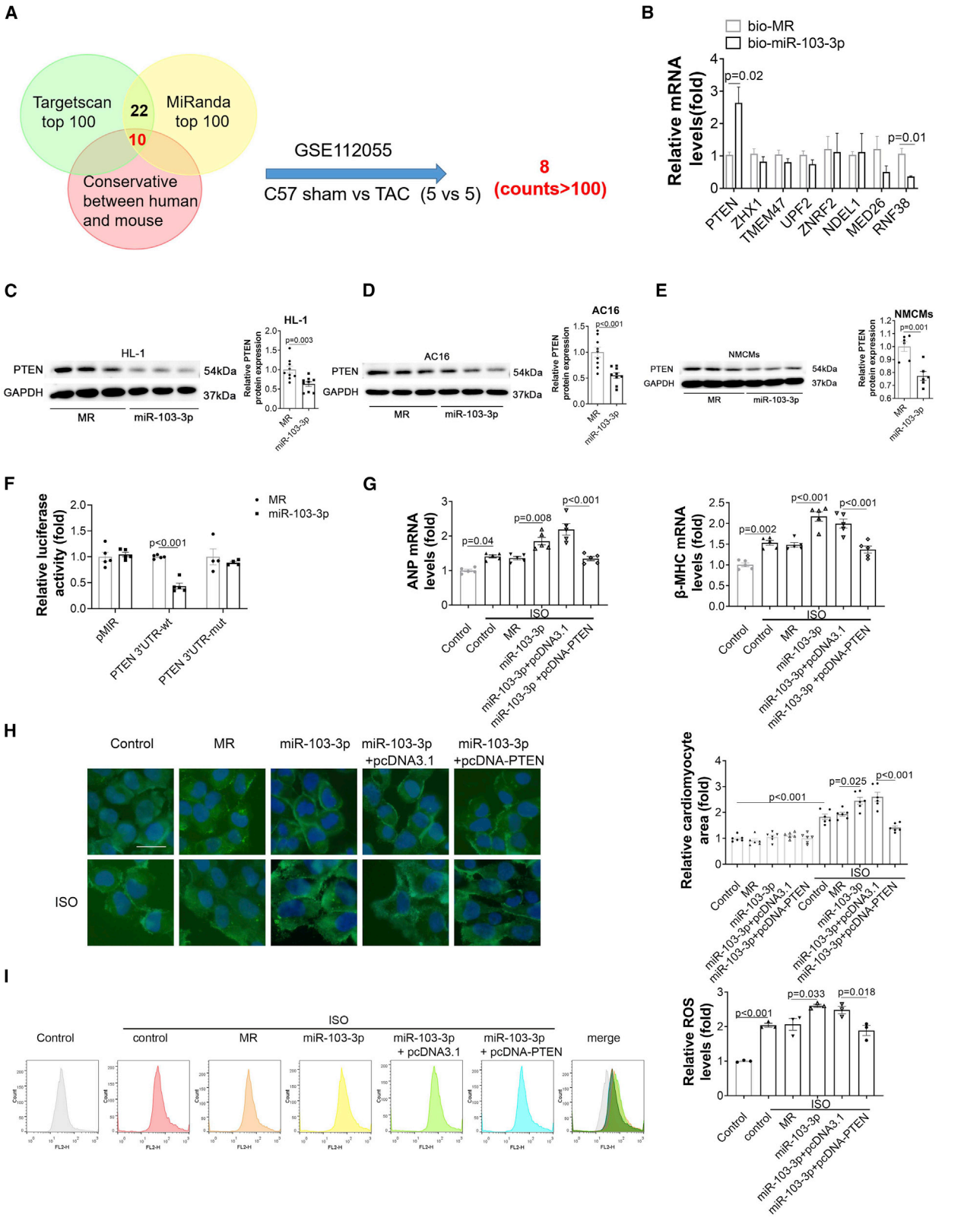

(legend on next page)

Overexpression of lnccytb ameliorated ISO-induced hypertrophy via the miR-103-3p/PTEN axis

To determine whether PTEN was the downstream target of lnccytb, we overexpressed lnccytb in HL-1 and AC16 cells. Based on our results, enhanced lnccytb expression could increase the protein levels of PTEN. Further, when pcDNA-lnccytb and miR-103-3p were co-transfected, the protein levels of PTEN were found to decrease relative to that achieved when pcDNA-lnccytb was co-transfected with MR in HL-1 and AC16 cells (Figures 6A and 6B). Western blot analysis of mouse heart tissue revealed that the overexpression of lnccytb augmented the protein levels of PTEN and inhibited the AKT phosphorylation at Ser473 *in vivo* (Figures 6C and 6D). In addition, the PTEN protein levels were positively correlated with the levels of lnccytb in TAC mouse hearts (Figure 6E). Knocking down PTEN expression increased hypertrophy marker expression and cardiomyocyte size when transfected with pcDNA-lnccytb (Figures 6F and 6G). Compared with the overexpression of lnccytb alone, knocking down PTEN expression was found to simultaneously increase ROS generation while co-transfected with pcDNA-lnccytb (Figure 6H). The efficiency of si-PTEN was also demonstrated via western blot (Figure S22).

Collectively, the overexpression of cytosolic lnccytb was found to mitigate cardiac hypertrophy and reduce ROS generation via the lnccytb/miR-103-3p/PTEN/AKT axis, ultimately improving HF (Figure 6I).

DISCUSSION

In the present study, we found that the expression of the mitochondrial-derived lncRNA, lnccytb, was reduced in the progression of HF. Moreover, this reduction was found to mainly occur in the cytosol. As a result, we proceeded to overexpress lnccytb in the cytosol, which improved cardiac function *in vivo* and *in vitro*. A further study indicated that lnccytb could act as a ceRNA to sponge miR-103-3p and relieve the suppressive effects exhibited by miR-103-3p on its downstream targets. Through mRNA sequencing and bioinformatics analysis, PTEN was identified to be the potential target of miR-103-3p. Thereafter, we demonstrated that lnccytb prevented hypertrophy and ROS activation, which led to the improvement of TAC-induced cardiac dysfunction. Mechanistically, *in vitro* study revealed that cytosol-localized lnccytb regulate myocyte phenotype and ROS production via the miR-103-3p/PTEN axis.

Numerous lncRNAs located in the nucleus or cytosol have been reported to be involved in the pathophysiology of HF. lncRNA ZFAS1 exists in both the nucleus and cytosol, causing intracellular Ca^{2+} overload and contractile dysfunction by acting as a SERCA2a inhibitor.[42] However, lncRNA Mhrt located in the cytosol could modulate cardiac hypertrophy via the miR-145a-5p/KLF4/myocardin axis.[43]

Recently, several studies have demonstrated that molecules derived from mitochondria play crucial roles in the pathophysiological process when exported to the cytosol. Cytosolic acetyl-coenzyme A (Ac-CoA), instead of the location of the mitochondria, was found to act as the leading metabolic modulator of autophagy.[44] Moreover, loss of mitochondrial one-carbon (1C) pathway in colon cancer could still promote tumorigenesis by cytosolic serine catabolism.[45] Meanwhile, mitochondria-located circular RNA SCAR could mitigate nonalcoholic steatohepatitis by reducing ROS generation.[46] Nevertheless, studies on mitochondrial-derived lncRNA in the cytosol are scarcely reported in HF.

Deep sequencing of human failing left ventricle (LV) samples and non-failing human LV samples indicated that 71% of the high-abundance lncRNAs were of mitochondrial origin.[47] Currently, several mitochondria-encoded lncRNAs have been validated, and human mitochondrial deep sequencing revealed that the abundance of lncND5, lncND6, and lnccytb was cell and tissue specific.[18] The levels of mitochondria-encoded SncmtRNA, ASncmtRNA-1, and ASncmtRNA-2 could be used to distinguish normal cells from cancer cells.[48] Using PacBio full-length transcriptome sequencing, two novel mitochondria-encoded lncRNAs, MDL1 and MDL1AS, were found to extensively exist in animal mitochondrial genomes.[49] However, only few studies on the function of these lncRNAs and the specific downstream pathways have been reported. In this study, we assumed that the subcellular distribution of mitochondrial lnccytb could be altered under stress. Although some ncRNAs could be exported to the cytosol, the concrete binding proteins or molecules are yet to be reported. For example, TERC, the RNA component of telomerase, could be imported into the mitochondria and cut into a shorter form called TERC-53, which returns to the cytosol.[50,51]

An important issue is why mitochondria-localized lnccytb failed to show any detectable changes in HF, considering that the translocation of lnccytb from the mitochondrial into the cytosol was impaired. In

Figure 5. miR-103-3p could target PTEN and promote hypertrophy

(A) Venn diagram showing the strategy to identify miRNAs downstream targets. (B) The levels of mRNA in miR-103-3p-transfected HL-1 cells detected by bio-miR-103-3p RIP ($n \geq 3$). (C) The protein levels of PTEN were detected by western blot analysis from differently treated HL-1 cells (left); quantitative analysis by ImageJ (right; n = 9). (D) The protein levels of PTEN were detected by western blot analysis in differently treated AC16 cells (left); quantitative analysis by ImageJ (right; n = 9). (E) The protein levels of PTEN were detected by western blot analysis in differently treated NMCMs (left); quantitative analysis by ImageJ (right; n = 6). (F) The binding of miR-103-3p with PTEN was detected by luciferase reporter assays in HEK293T cells ($n > 3$). (G) Expression levels of ANP and β-MHC mRNA in AC16 cardiomyocytes with different treatments measured by real-time PCR (n = 5). (H) Representative images of cardiomyocyte areas stained by phalloidin (green) and Hoechst (blue) (left). Scale bar, 50 μm. Quantitative analysis of cell sizes by Image-Pro Plus is shown (right). (I) ROS levels were stained by DHE probe in AC16 cells with different treatments detected by flow cytometry (n = 3; left); quantitative analysis of flow cytometry data (right). (B and F) Student's t test; (C and E) comparisons of parameters were performed with Mann-Whitney U test. (G–I) One-way ANOVA followed by the Tukey's post hoc analysis was used. Data are expressed as mean ± SEM.

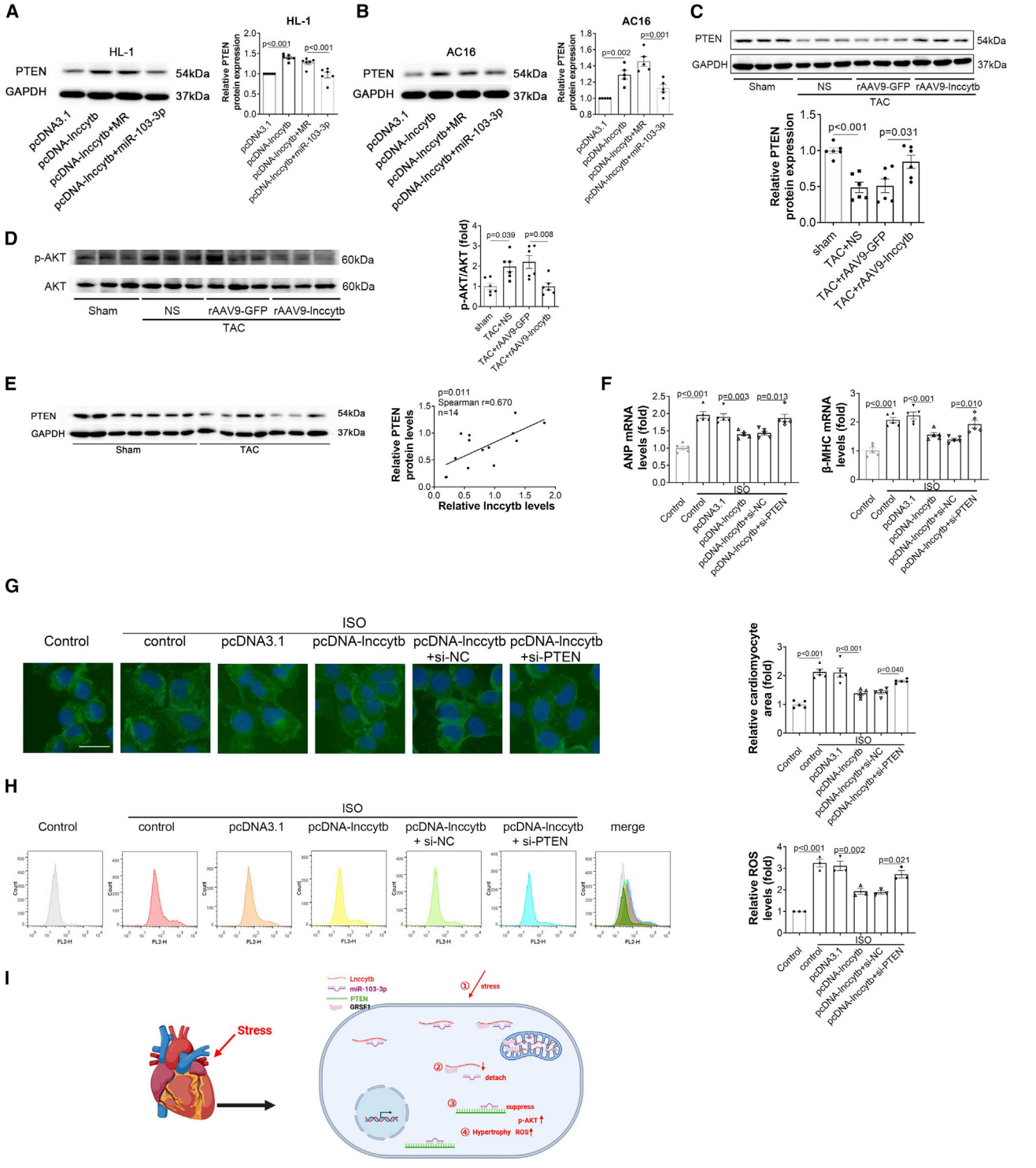

Figure 6. Overexpression of lnccytb ameliorated hypertrophy and ROS generation caused by ISO via lnccytb/miR-103-3p/PTEN axis

(A) The representative images of PTEN were detected by western blot in HL-1 cells with overexpression of lnccytb and miR-103-3p (left), quantitatively analyzed by ImageJ (right; n = 6). (B) The representative images of PTEN were detected by western blot in AC16 cells with overexpression of lnccytb and miR-103-3p (left), quantitatively analyzed by ImageJ (right; n = 5). (C) The protein levels of PTEN were tested by western blot analysis in mice heart tissues (up), quantitatively analyzed by ImageJ (down; n = 6 per group). (D) The protein levels of p-AKT (Ser-473) and total AKT were measured by western blot in mice heart tissues (left), quantitatively analyzed by ImageJ (right; n = 6 per

(legend continued on next page)

fact, GRSF1 is the key protein of mitochondrial RNA granules, being widely involved in mitochondrial RNA processing, posttranscriptional regulation, and degradation.[52–54] However, all of these studies have been performed through *in vitro* or *ex vivo* approaches due to the lack of GRSF1 transgenic mice.[55] In this study, RNA pull-down assay and protein MS were used to find the interaction proteins with lnccytb in mitochondria and cytosol. Western blotting and knockdown assay also indicated that GRSF1 could export lnccytb from mitochondria to cytosol. We reasoned that the level of mitochondrial-localized lnccytb was determined by (1) the synthesis of lnccytb and (2) the translocation efficiency of lnccytb into the cytosol. Because the global level of lnccytb was decreased (Figures 1E and 1F), the unchanged lnccytb level in the mitochondria might be explained by the dynamic balance between decreased synthesis and impaired exporting efficiency. We have provided this hypothesis model as Figure S19E.

The relatively low conservation of lncRNAs increased the translation difficulty between animal models and human diseases.[3] However, mitochondrial lncRNA alleviated the gap of conservation owing to evolution. The relatively high conservation of lnccytb suggested a promising clinical significance.

In addition, the overexpression of the coding strand, cytb, did not affect TAC-induced cardiac dysfunction. This outcome may be attributed to the specific tRNAs and genetic codes in the mitochondria,[10,56] which prevented cytb protein expression in the cytosol. Further, the cytb mRNA transcripts and cytb protein were specifically expressed in the mitochondria (Figure S23A), as previously described.[12] According to the universal genetic code, when mitochondrial ND6 was added to the N-terminal mitochondrial targeting and the hemagglutinin (HA) epitope, the allotropically expressed ND6 could not be internalized by the mitochondria.[57]

miR-103 was reported to be involved in the process of multiple diseases. miR-103/107 could increase insulin sensitivity and ameliorate glucose homeostasis via inhibiting caveolin-1 in obese mice.[58] However, the systematic inhibition of miR-103/107 decreased cardiac function and mitochondrial oxidative capacity without pathological stimuli.[59] Considering that the targets in liver tissues of miR-103/107 were regulated by using the global inhibitors, there might be crosstalk between the liver and the heart. In the progression of atherosclerosis, miR-103 of endothelial cells could promote inflammation and endoplasmic reticulum (ER) stress via blocking PTEN-mediated mitogen-activated protein kinase (MAPK) signaling.[60] Here, we demonstrated that miR-103-3p was a target of lnccytb in TAC-induced heart failure. Meanwhile, overexpression of miR-103-3p could enhance cardiac hypertrophy by inhibiting PTEN expression.

The marked imbalance in energy demand and supply was considered to be one of the causes of HF. Moreover, ROS was reported to promote sudden cardiac death and cause chronic proteome remodeling in HF.[61] In this study, we measured the levels of elevated ROS in the process of HF and found that overexpressed cytosolic lnccytb could reduce ROS *in vivo* and *in vitro*. In addition, a series of studies have suggested that PTEN can be regulated by cellular ROS. Cellular PTEN activity is suppressed by ROS-induced oxidation of active-site cysteine,[62] and peroxidase peroxiredoxin1 (Prdx1) can prevent PTEN from ROS-induced inactivation via binding to it.[63] Meanwhile, overexpression of PTEN could also inhibit ROS generation. Circular RNA circNR3C1 decreased intracellular ROS production by enhancing PTEN expression and subsequently inhibiting AKT/mTOR pathway.[64] Aside from ROS generation, PTEN is involved in cardiac hypertrophy signaling. PTEN is able to be a negative regulator of the phosphatidylinositol 3-kinase (PI3K)/AKT pathway to suppress glycolysis, induce autophagy, and impede cardiac hypertrophy.[65–67] Here, we found that the overexpression of cytosolic lnccytb could alleviate TAC-induced HF and lower ROS generation by directly sponging miR-103-3p to enhance PTEN expression.

In HF, lnccytb and its downstream targeting gene PTEN were both decreased. Theoretically, targeting lnccytb and PTEN should be able to achieve the similar therapeutic effects. However, PTEN itself was involved in tumor progress and metabolic regulation as a negative regulator of PI3K/AKT signaling pathway.[68] Therefore, sustained PTEN overexpression by rAAV9 might lead to some unwanted adverse effects, such as carcinogenesis and metabolic disturbance. In contrast, by targeting lnccytb, PTEN level was stringently regulated to avoid overdosage. In other words, lnccytb overexpression protected against the downregulation of PTEN in HF and restored PTEN to its physiological function.

In addition, we then performed longitudinal analysis for a cohort of heart failure patients along the progression or recovery from post-myocardial infarction (MI) patients during acute versus compensated states following reperfusion. Specifically, we recruited 20 patients with acute MI followed by percutaneous coronary intervention (PCI) treatment. The characteristics of the patients were listed in Table S7. The plasma samples from the pre-PCI and post-PCI of these patients were collected. Interestingly, we found that circulating levels of lnccytb were dramatically increased after PCI treatment (Figure S24A). The dynamic expression pattern of circulating lnccytb

group). (E) The protein levels of PTEN were measured by western blot in sham and TAC mice heart tissues (left); the correlation between cardiac PTEN protein level and lnccytb level was analyzed in mouse heart (right). Sham (n = 7); TAC (n = 7). (F) Expression of ANP (left) and β-MHC (right) mRNA in AC16 cardiomyocytes with overexpression of lnccytb and downregulation of PTEN, measured by real-time PCR (n = 5). (G) Representative images of cardiomyocyte areas stained by phalloidin (green) and Hoechst (blue) (left). Scale bar, 50 μm. Quantitative analysis of cell sizes by Image-Pro Plus is shown (right). (H) ROS levels were stained by DHE probe in AC16 cells with overexpression of lnccytb and downregulation of PTEN, detected by flow cytometry (n = 3; left); quantitative analysis of flow cytometry data (right). (I) A model diagram to illustrate the role of lnccytb in HF. Cardiac stress increased miR-103-3p by inhibiting the expression lnccytb, which caused the reduction of PTEN, leading to enhancement of ROS and cardiac dysfunction. (A–D and F–H) One-way ANOVA followed by the Tukey's post hoc analysis was used. Data are expressed as mean ± SEM.

over the disease course suggested strong diagnostic and prognostic potential for lnccytb in cardiac diseases.

This study had some limitations. First, based on high-throughput sequencing, lnccytb was expected to sponge several miRNAs and not just miR-103-3p. Our data have indicated that overexpression of lnccytb could not totally block down the effects of miR-103-3p and suggested that miR-103-3p might have multiple targets. During the progression of HF, lnccytb was reduced, to some extent, in the mitochondria. Meanwhile, our results have presented that the mRNA and protein of cytb were also reduced in HF. Considering that cytb was mainly located in the mitochondria, there might be different degradation mechanisms compared with cytosolic fractions. Meanwhile, the gene expressions of light strand and heavy strand were affected by strand-biased mitochondrial DNA methylation.[69] Although the mtDNA copy numbers were not changed by TAC operation, the expression of cytb RNA could still be reduced. Further, a small stem-loop structure of the mitochondria-targeted RNA was reported to import RNA into the mitochondria.[51,70] Therefore, we opted to construct the same stem loop sequence with lnccytb. However, we could only detect increments of lnccytb expression in the cytosol and not in the mitochondria (Figure S25A). Such finding indicates that a more complicated three-dimensional structure might be needed to import RNAs into the mitochondria. The studies mentioned previously were conducted using *in vitro* RNA import assays; however, the real conditions in organisms might be more sophisticated. Moreover, we could not apply the classical mitochondria-targeted coding sequence, such as Su9,[71] owing to the noncoding character of lncRNAs. It was recently revealed that an RNA sequence longer than 77 nt could not be imported into the mitochondria,[72] thereby indicating the limitation of the current technology.

Collectively, we demonstrated that cytosolic lnccytb could function as a ceRNA to improve cardiac function in HF through the lnccytb/miR-103-3p/PTEN/AKT axis.

MATERIALS AND METHODS

Reagents

Dulbecco's modified Eagle's medium (DMEM) and fetal bovine serum (FBS) were purchased from Gibco (Grand Island, NY). Lipofectamine 2000 (Lipo2000) reagent was obtained from Invitrogen (Carlsbad, CA). miR-103-3p mimics, miR-103-3p inhibitor, biotin-labeled miR-103-3p, and antisense oligonucleotide (ASO) for lnccytb were purchased from RiboBio (Guangzhou, China). The primers of miR-103-3p and U6 were also acquired from RiboBio (Guangzhou, China). Real-time PCR primers for mRNA were synthesized by Augct (Wuhan, China). Antibodies against GFP (cat. no. AE012), VDAC1 (cat. no. A15735), and PTEN (cat. no. A19104) were purchased from ABclonal (Wuhan, China). Anti-GAPDH (cat. no. 60004-1-Ig) and anti-ANP (cat no. 27426-1-AP) were purchased from Proteintech (Chicago, IL). Phospho-Akt (Ser473) (cat. no. 4060) and Akt (cat. no. 4691) were purchased from Cell Signaling Technology (Beverly, MA). Polyvinylidene difluoride (PVDF) membranes were purchased from Millipore (Darmstadt, Germany). FITC-phalloidin (cat. no. P5282) and other chemical reagents were purchased from Sigma-Aldrich (Shanghai, China). Adeno-associated virus (AAV) and adeno virus were purchased from WZ Biosciences (Shandong, China).

Construction of recombinant adeno-associated virus (rAAV)

We used the rAAV system (type 9) to manipulate the expression of cytb mRNA and lnccytb *in vivo*. The rAAV system was a gift from Dr. Xiao (East China University of Science and Technology, China). The sequence of mouse lnccytb was identified using RACE assays. The rAAVs were packaged by triple plasmid co-transfection, as described previously.[73]

Human plasma and heart tissue samples

Plasma samples were obtained from another population of 11 non-HF controls and 12 HF patients; the baseline characteristics are listed in Table S5. The left ventricular tissues from eight patients diagnosed with end-stage HF were collected during heart transplantation. Control heart specimens (n = 6) were acquired from donors who died in accidents. All donor grafts were donated following brain death to the Red Cross Society and allocated by the China Organ Transplant Response System, according to Chinese laws;[74] this population was derived from our published article.[75] The characteristics of the controls and patients are listed in Table S6. All procedures involving human specimens were authorized by the ethics committee of Tongji Hospital and Tongji Medical College. All programs complied with the principles outlined in the Declaration of Helsinki. All participants were aware of the nature of the study and gave written consent for their participation.

Animals

The research was approved by the Institutional Animal Research Committee of Tongji Medical College. All animal experimental protocols were performed according to the US National Institutes of Health guidelines for the Care and Use of Laboratory Animals. Male C57BL/6 mice (age, 8 weeks old) were purchased from the Experimental Animal Center of Hubei (Wuhan, China). To manipulate the expression levels of cytb mRNA and lnccytb, mice were randomly divided into the following groups: sham, TAC, TAC + rAAV9-GFP, TAC + rAAV9-cytb, and TAC + rAAV9-lnccytb (n = 10/group). Each mouse received a single intravenous injection of 1×10^{11} corresponding virion particles in 100 μL of saline solution via the tail vein after 2 weeks of TAC operation. For preventative effect, 2 weeks after virus injection, mice were anesthetized with pentobarbital (60 mg/kg, intraperitoneal injection) and mechanically ventilated with a tidal volume of 0.2 mL and a respiratory rate of 100 breaths per minute, and then TAC was applied to induce pressure-overload-induced cardiac hypertrophy as previously reported.[76] Moreover, to figure out whether lnccytb could affect the cardiac function under normal condition, mice were randomly divided into the following groups: control, rAAV9-GFP, rAAV9-cytb, rAAV9-lnccytb, AAV9-sh-GFP, and AAV9-sh-lnccytb (n = 5/group).

In addition, to evaluate the effect of lnccytb knockdown, mice were randomly divided into the following groups: sham, TAC, TAC +

AAV9-sh-GFP, and TAC + AAV9-sh-lnccytb (n = 10/group). After 2 weeks of TAC operation, these mice were injected into the same titer of virus.

Tissue harvesting

Eight weeks after the operation, all animals were profoundly anesthetized via an intraperitoneal injection of sodium pentobarbital (60 mg/kg) and sacrificed by exsanguination (section of the descending abdominal aorta). After harvesting, the tissue samples were placed immediately in ice-cold PBS, cleaned and frozen in liquid nitrogen, and stored at −80°C.

Echocardiography and hemodynamics

Echocardiography analysis was carried out using a 30-MHz high-frequency scanhead (VisualSonics Vevo770, VisualSonics, Toronto, Canada) as described previously.[77] Hemodynamic measurements were performed using a Millar Catheter System (Millar 1.4F, SPR835, Millar Instruments, Houston, TX) as described previously.[78]

Cell culture and transfection

The human cardiomyocyte line, AC16, and HEK293T were obtained from American Type Culture Collection (ATCC) (Manassas, VA) and cultured in DMEM supplemented with 10% FBS. Mouse atrial cardiomyocyte tumor lineage HL-1 cells were also purchased from ATCC (Manassas, VA) and cultured in Claycomb Medium (Sigma, Shanghai, China) with 4 mM L-glutamine (Sigma, Shanghai, China), 100 μM norepinephrine (Sigma, Shanghai, China), and 10% FBS. Cells were cultured at 37°C under a relative humidity of 95% in a 5% CO_2 atmosphere.

Cells were transfected with miR-103-3p mimics (100 nM), miR-103-3p inhibitor (100 nM), or their negative control (100 nM), according to the manufacturer's protocol for Lipo2000 (Invitrogen, Carlsbad, CA). ISO was used to treat cells for 24 h at 10 μM final concentration.

Mitochondria isolation

The mitochondria of cultured cells were isolated according to the instruction of the Mitochondria Isolation Kit for Cultured Cells from Thermo Fisher Scientific (cat. no. 89874). The mitochondria from mouse heart tissues were extracted using the MACS Mitochondria Extraction Kit from Miltenyi Biotec (cat. no. 130-097-340), according to the manufacturer's protocol. Briefly, cells were lysed and the mitochondria were magnetically captured with anti-TOM22 antibody-coated beads. The eluted mitochondria were collected by centrifugation at 13,000 × *g* for 2 min at 4°C, as described previously.[11]

Quantification of ROS production

DHE staining (Invitrogen, Carlsbad, CA) was performed to measure intracellular ROS production in myocardial tissues, according to the manufacturer's instructions. Fluorescence intensity was measured under a Nikon DXM1200 fluorescence microscope and analyzed using Image-Pro software (Media Cybernetics, Bethesda, MD). To evaluate intracellular ROS production *in vitro*, AC16 cells were incubated with DHE (Invitrogen, Carlsbad, CA). To evaluate mitochondrial ROS production *in vitro*, AC16 cells were incubated with MitoSOX-RED probe (Yeason, Shanghai, China). After incubation, cells were measured using a FACStar Plus flow cytometer (BD Biosciences, Sparks, MD), as previously described.[12]

RNA isolation and semiquantitative and absolute quantification by real-time PCR

Total RNA was acquired using TRIzol (Invitrogen, Carlsbad, CA) and reverse transcribed to cDNA using the first-strand cDNA synthesis kit (Thermo Scientific, Carlsbad, CA), according to the manufacturer's instructions. Strand-specific quantitative real-time PCR was performed as described previously, except that the Taqman-specific probes were used to detect the human and mouse lnccytb transcripts.[30] The expression levels of miR-103-3p and mRNA were quantified by quantitative real-time PCR using the SYBR Select Master Mix (Life Technologies, Carlsbad, CA) based on a 7900HT FAST real-time PCR system (Life Technologies, Carlsbad, CA). U6 was employed as an endogenous control to miRNA while GAPDH was used as endogenous control to mRNA. 18S ribosome RNA was used as endogenous control to lnccytb. Each sample had three replicate measurements. Relative expression levels were analyzed by the $2^{-\Delta\Delta ct}$ method, as previously described.[11]

Absolute quantitative real-time PCR was performed as previously described.[79] A standard curve was generated according to a previous reference.[46] Briefly, linear mouse lnccytb and human lnccytb were cloned into the pcDNA3.1 vector with a T7 promoter. RNA was transcribed *in vitro* using TranscriptAid T7 High Yield Transcription Kit (cat. no. K0441, Thermo Fisher Scientific). Standard curve was generated via series dilution of *in vitro* transcribed linear human lnccytb RNA with a molecular weight of 387,840 g/mol and mouse lnccytb RNA with molecular a weight of 367,680 g/mol. Data are presented as copies per 20 pg total RNA. At least three experimental replicates were performed.

miRNA absolute quantitative real-time PCR was based on the standard curve by standard miRNA (cat. no. R10033.1, RiboBio, Guangzhou, China). Briefly, standard miR-103-3p was diluted into multiple concentrations and reverse transcribed to cDNA together with the cell RNA (corresponding to RNA derived from 0.1 million cells). Finally, standard curve was produced by Ct value and Log_{10}(copies).

The sequences of probes for mRNA detection are listed in Table S8, while the sequences of the Taqman probes for strand-specific qPCR detection are listed in Table S9.

5′ and 3′ rapid cDNA end amplification (RACE)

5′ and 3′ RACE were performed to identify the full-length transcript of mouse lnccytb in accordance with the SMARTer RACE 5′/3′ Kit (Clontech, Fremont, CA). Briefly, a gene-specific RACE product was produced via PCR amplification. Thereafter, the products were cloned following the In-Fusion strategy (Clontech, Fremont, CA). Finally, the inserts cloned into plasmids were sequenced to identify the 5′ and 3′ ends of lncRNA cytb. The primer sequences are listed in Table S10.

Northern blot analysis

Northern blot was performed as previously described.[80] Briefly, the samples were run on a 15% polyacrylamide-urea gel and subsequently transferred to positively charged nylon membranes (Millipore) followed by cross-linking through UV irradiation. The membranes were hybridized with 100 pmol 3′-digoxigenin (DIG)-labeled probes overnight at 42°C. Probes labeled with DIG were synthesized by Sangon Biotech (Shanghai, China). The probe sequence for lnccytb is listed in Table S5.

RNA fluorescence *in situ* hybridization (FISH) and double FISH

FISH was performed as described previously.[81] Briefly, paraffin-embedded mouse heart tissues were sectioned into 4-mm-thick slices. The heart sections also underwent deparaffinization and rehydration and antigen unmasking. Thereafter, they were washed three times with 1× PBS, incubated with pre-hybridization buffer at 55°C for 30 min, and then incubated with the digoxin-labeled probe at 55°C for 1 h in hybridization buffer. After incubation with the lnccytb probe and Cy3-labeled antisense miR-103-3p, heart sections were washed and treated with anti-DIG antibody (PerkinElmer, Waltham, MA) for 1 h at 37°C. Tyramide signal amplification (PerkinElmer, Waltham, MA) was applied to improve FISH detection. The mitochondrial marker Tom20 antibody (1:50) and Hoechst were applied to the cardiomyocytes or sectioned heart and processed for confocal imaging.

RNA pull-down

Biotinylated miR-103-3p mimic or control miRNA was transfected into HL-1 cells for 48 h. Cells were then harvested, and streptavidin-labeled magnetic beads were used to bind biotinylated miR-103-3p. After elution from the beads, bound RNA was extracted with TRIzol and quantified by real-time real-time PCR.

In vitro biotin-labeled RNA (lnccytb) was synthesized by *in vitro* transcription with kit from Thermo Fisher Scientific (cat. no. K0441). In brief, PCR fragments were amplified with forward primers containing T7 RNA polymerase promoter sequence. Purified PCR products were used as a DNA template for *in vitro* transcription. Then, the target RNA was biotinylated at the 3′ end using the Thermo Fisher Scientific Pierce RNA 3′ Biotinylation Kit (cat. no. 20163). Whole sham mouse heart tissue lysates were incubated with purified biotinylated RNA probes. RNA-protein complexes were further isolated by Thermo Fisher Scientific Pierce Magnetic RNA-Protein Pull-Down Kit (cat. no. 20164). The recruited proteins were detected by LC-MS or western blot.

lncRNA prediction and miRNA target prediction

The bioinformatics website, RegRNA2.0 (http://regrna2.mbc.nctu.edu.tw/), was used to predict the miRNAs that bind with lnccytb, while TargetScan (http://www.targetscan.org) and miRanda (http://www.miranda.org/) were used to predict the miRNA targets.

mRNA sequencing (mRNA-seq)

RNA-seq and analyses of the results were conducted by Personal Biotechnology (Shanghai, China). The threshold value for significance was a fold change >2 with a $p < 0.05$.

Western blotting

Western blotting was performed with specific antibodies, as previously described.[82] The intensities of individual bands were analyzed by densitometry using ImageJ (National Institutes of Health Software, Bethesda, MD) and normalized to the level of GAPDH.

Fluorescein isothiocyanate (FITC)-phalloidin staining

AC16 cells were washed three times with PBS, fixed in 4% paraformaldehyde for 15 min, and incubated with 0.1% Triton X-100 for 15 min. Thereafter, the cells were incubated in FITC-phalloidin at 4°C overnight away from the light. Images were captured with a Nikon DXM1200 fluorescence microscope, and quantification was performed using Image-Pro Plus v.6.0 software (Media Cybernetics, Bethesda, MD).

Co-immunoprecipitation with anti-GFP antibody

HL-1 cells were co-transfected with pcDNA3.1-MS2, pcDNA3.1-MS2-lnccytb, pcDNA3.1-MS2-lnccytb-mut, and pMS2-GFP (Addgene). After 48 h, cells were used to perform RIP experiments using a GFP antibody, as previously described.[83] The remaining products were extracted with TRIzol, and the levels of mRNA were quantified by real-time PCR.

Dual luciferase assay

For the dual luciferase assay, 400 ng of pMIR-PTEN 3′ UTR, pMIR-PTEN 3′ UTR mutant, or the empty vector was transfected into HEK293T cells with 40 ng of pRL-TK plasmid (Promega, Madison, WI). The miR-103-3p mimics or miRNA random was co-transfected with those reporter plasmids at a final concentration of 100 nM. After 48 h, luciferase activity was detected with a Dual-Luciferase Reporter Assay System (Promega, Madison, WI), according to the manufacturer's protocol.

Statistical analysis

Data are presented as mean ± SEM. Statistical comparisons were made by two-tailed unpaired Student's t test for two groups or one-way analysis of variance (ANOVA) followed by the Tukey post hoc analysis for three groups or more. If the data distribution failed normality by the Shapiro-Wilk test, the Mann-Whitney U test for two groups was performed. All calculations were performed using Prism (v.8; GraphPad Software, La Jolla, CA). $p < 0.05$ was considered significant.

SUPPLEMENTAL INFORMATION

Supplemental information can be found online at https://doi.org/10.1016/j.omtn.2022.02.002.

ACKNOWLEDGMENTS

This work was supported by a grant from the National Natural Science Foundation of China (nos. 81822002, 31771264, 82170273, 31800973, 81630010, 81790624, and 82000387) and the Fundamental Research Funds for the Central Universities (2019kfyXMBZ035). The funders had no role in study design, data collection and analysis, decision to publish, or preparation of the manuscript.

AUTHOR CONTRIBUTIONS

X.Z. and S.Y. designed the study, analyzed and interpreted the data, and drafted the paper; J.L., Y.T., Y.W., J.Z., J.F., X.N., Y.Z., Z.W., and H.L. participated in acquiring the data; and C.C. and D.W.W. designed the work and drafted the paper.

DECLARATION OF INTERESTS

The authors declare no competing interests.

REFERENCES

1. Rossignol, P., Hernandez, A.F., Solomon, S.D., and Zannad, F. (2019). Heart failure drug treatment. Lancet *393*, 1034–1044.
2. Normand, C., Kaye, D.M., Povsic, T.J., and Dickstein, K. (2019). Beyond pharmacological treatment: an insight into therapies that target specific aspects of heart failure pathophysiology. Lancet *393*, 1045–1055.
3. Gomes, C.P.C., Schroen, B., Kuster, G.M., Robinson, E.L., Ford, K., Squire, I.B., Heymans, S., Martelli, F., Emanueli, C., and Devaux, Y. (2020). Regulatory RNAs in heart failure. Circulation *141*, 313–328.
4. Luongo, T.S., Lambert, J.P., Gross, P., Nwokedi, M., Lombardi, A.A., Shanmughapriya, S., Carpenter, A.C., Kolmetzky, D., Gao, E., van Berlo, J.H., et al. (2017). The mitochondrial Na(+)/Ca(2+) exchanger is essential for Ca(2+) homeostasis and viability. Nature *545*, 93–97.
5. Wang, B., Nie, J., Wu, L., Hu, Y., Wen, Z., Dong, L., Zou, M.H., Chen, C., and Wang, D.W. (2018). AMPKα2 protects against the development of heart failure by enhancing mitophagy via PINK1 phosphorylation. Circ. Res. *12*, 712–729.
6. Virani, S.S., Alonso, A., Benjamin, E.J., Bittencourt, M.S., Callaway, C.W., Carson, A.P., Chamberlain, A.M., Chang, A.R., Cheng, S., Delling, F.N., et al. (2020). Heart disease and stroke statistics-2020 update: a report from the American heart association. Circulation *141*, e139–e596.
7. van der Bliek, A.M., Sedensky, M.M., and Morgan, P.G. (2017). Cell biology of the mitochondrion. Genetics *207*, 843–871.
8. Rajendran, J., Purhonen, J., Tegelberg, S., Smolander, O.P., Morgelin, M., Rozman, J., Gailus-Durner, V., Fuchs, H., Hrabe de Angelis, M., Auvinen, P., et al. (2019). Alternative oxidase-mediated respiration prevents lethal mitochondrial cardiomyopathy. EMBO Mol. Med. *11*, e9456.
9. Gusic, M., Schottmann, G., Feichtinger, R.G., Du, C., Scholz, C., Wagner, M., Mayr, J.A., Lee, C.Y., Yepez, V.A., Lorenz, N., et al. (2020). Bi-allelic UQCRFS1 variants are associated with mitochondrial complex III deficiency, cardiomyopathy, and alopecia totalis. Am. J. Hum. Genet. *106*, 102–111.
10. Hällberg, B.M., and Larsson, N.G. (2014). Making proteins in the powerhouse. Cell Metab. *20*, 226–240.
11. Li, H., Zhang, X., Wang, F., Zhou, L., Yin, Z., Fan, J., Nie, X., Wang, P., Fu, X.D., Chen, C., et al. (2016). MicroRNA-21 lowers blood pressure in spontaneous hypertensive rats by upregulating mitochondrial translation. Circulation *134*, 734–751.
12. Li, H., Dai, B., Fan, J., Chen, C., Nie, X., Yin, Z., Zhao, Y., Zhang, X., and Wang, D.W. (2019). The different roles of miRNA-92a-2-5p and let-7b-5p in mitochondrial translation in db/db mice. Mol. Ther. Nucleic Acids *17*, 424–435.
13. Yao, R.W., Wang, Y., and Chen, L.L. (2019). Cellular functions of long noncoding RNAs. Nat. Cell Biol. *21*, 542–551.
14. Han, P., Li, W., Lin, C.H., Yang, J., Shang, C., Nuernberg, S.T., Jin, K.K., Xu, W., Lin, C.Y., Lin, C.J., et al. (2014). A long noncoding RNA protects the heart from pathological hypertrophy. Nature *514*, 102–106.
15. Yu, J., Yang, Y., Xu, Z., Lan, C., Chen, C., Li, C., Chen, Z., Yu, C., Xia, X., Liao, Q., et al. (2020). Long noncoding RNA ahit protects against cardiac hypertrophy through SUZ12 (suppressor of zeste 12 protein homolog)-mediated downregulation of MEF2A (myocyte enhancer factor 2A). Circ. Heart Fail. *13*, e006525.
16. Lv, L., Li, T., Li, X., Xu, C., Liu, Q., Jiang, H., Li, Y., Liu, Y., Yan, H., Huang, Q., et al. (2018). The lncRNA Plscr4 controls cardiac hypertrophy by regulating miR-214. Mol. Ther. Nucleic Acids *10*, 387–397.
17. Mercer, T.R., Neph, S., Dinger, M.E., Crawford, J., Smith, M.A., Shearwood, A.M., Haugen, E., Bracken, C.P., Rackham, O., Stamatoyannopoulos, J.A., et al. (2011). The human mitochondrial transcriptome. Cell *146*, 645–658.
18. Rackham, O., Shearwood, A.M., Mercer, T.R., Davies, S.M., Mattick, J.S., and Filipovska, A. (2011). Long noncoding RNAs are generated from the mitochondrial genome and regulated by nuclear-encoded proteins. RNA *17*, 2085–2093.
19. Haddadi, N., Lin, Y., Travis, G., Simpson, A.M., Nassif, N.T., and McGowan, E.M. (2018). PTEN/PTENP1: 'Regulating the regulator of RTK-dependent PI3K/Akt signalling', new targets for cancer therapy. Mol. Cancer *17*, 37.
20. Vitiello, M., Evangelista, M., Zhang, Y., Salmena, L., Pandolfi, P.P., and Poliseno, L. (2020). PTENP1 is a ceRNA for PTEN: it's CRISPR clear. J. Hematol. Oncol. *13*, 73.
21. Lai, J.H., Wang, M.Y., Huang, C.Y., Wu, C.H., Hung, L.F., Yang, C.Y., Ke, P.Y., Luo, S.F., Liu, S.J., and Ho, L.J. (2018). Infection with the dengue RNA virus activates TLR9 signaling in human dendritic cells. EMBO Rep. *19*, e46182.
22. Landerer, E., Villegas, J., Burzio, V.A., Oliveira, L., Villota, C., Lopez, C., Restovic, F., Martinez, R., Castillo, O., and Burzio, L.O. (2011). Nuclear localization of the mitochondrial ncRNAs in normal and cancer cells. Cell Oncol. *34*, 297–305.
23. Kumarswamy, R., Bauters, C., Volkmann, I., Maury, F., Fetisch, J., Holzmann, A., Lemesle, G., de Groote, P., Pinet, F., and Thum, T. (2014). Circulating long noncoding RNA, LIPCAR, predicts survival in patients with heart failure. Circ. Res. *114*, 1569–1575.
24. Landgraf, P., Rusu, M., Sheridan, R., Sewer, A., Iovino, N., Aravin, A., Pfeffer, S., Rice, A., Kamphorst, A.O., Landthaler, M., et al. (2007). A mammalian microRNA expression atlas based on small RNA library sequencing. Cell *129*, 1401–1414.
25. Natarelli, L., Geißler, C., Csaba, G., Wei, Y., Zhu, M., di Francesco, A., Hartmann, P., Zimmer, R., and Schober, A. (2018). miR-103 promotes endothelial maladaptation by targeting lncWDR59. Nat. Commun. *9*, 2645.
26. Wang, J.X., Zhang, X.J., Li, Q., Wang, K., Wang, Y., Jiao, J.Q., Feng, C., Teng, S., Zhou, L.Y., Gong, Y., et al. (2015). MicroRNA-103/107 regulate programmed necrosis and myocardial ischemia/reperfusion injury through targeting FADD. Circ. Res. *117*, 352–363.
27. Shi, J., Bei, Y., Kong, X., Liu, X., Lei, Z., Xu, T., Wang, H., Xuan, Q., Chen, P., Xu, J., et al. (2017). miR-17-3p contributes to exercise-induced cardiac growth and protects against myocardial ischemia-reperfusion injury. Theranostics *7*, 664–676.
28. Chen, C., Zou, L.X., Lin, Q.Y., Yan, X., Bi, H.L., Xie, X., Wang, S., Wang, Q.S., Zhang, Y.L., and Li, H.H. (2019). Resveratrol as a new inhibitor of immunoproteasome prevents PTEN degradation and attenuates cardiac hypertrophy after pressure overload. Redox Biol. *20*, 390–401.
29. Xie, X., Wang, H.X., Li, N., Deng, Y.W., Bi, H.L., Zhang, Y.L., Xia, Y.L., and Li, H.H. (2020). Selective inhibition of the immunoproteasome β5i prevents PTEN degradation and attenuates cardiac hypertrophy. Front. Pharmacol. *11*, 885.
30. Antonicka, H., Sasarman, F., Nishimura, T., Paupe, V., and Shoubridge, E.A. (2013). The mitochondrial RNA-binding protein GRSF1 localizes to RNA granules and is required for posttranscriptional mitochondrial gene expression. Cell Metab. *17*, 386–398.
31. Liang, H., Pan, Z., Zhao, X., Liu, L., Sun, J., Su, X., Xu, C., Zhou, Y., Zhao, D., Xu, B., et al. (2018). LncRNA PFL contributes to cardiac fibrosis by acting as a competing endogenous RNA of let-7d. Theranostics *8*, 1180–1194.
32. Yu, C., Li, L., Xie, F., Guo, S., Liu, F., Dong, N., and Wang, Y. (2018). LncRNA TUG1 sponges miR-204-5p to promote osteoblast differentiation through upregulating Runx2 in aortic valve calcification. Cardiovasc. Res. *114*, 168–179.
33. Sumazin, P., Yang, X., Chiu, H.S., Chung, W.J., Iyer, A., Llobet-Navas, D., Rajbhandari, P., Bansal, M., Guarnieri, P., Silva, J., et al. (2011). An extensive microRNA-mediated network of RNA-RNA interactions regulates established oncogenic pathways in glioblastoma. Cell *147*, 370–381.
34. Thomson, D.W., and Dinger, M.E. (2016). Endogenous microRNA sponges: evidence and controversy. Nat. Rev. Genet. *17*, 272–283.
35. Denzler, R., Agarwal, V., Stefano, J., Bartel, D.P., and Stoffel, M. (2014). Assessing the ceRNA hypothesis with quantitative measurements of miRNA and target abundance. Mol. Cell *54*, 766–776.
36. Paraskevopoulou, M.D., Georgakilas, G., Kostoulas, N., Reczko, M., Maragkakis, M., Dalamagas, T.M., and Hatzigeorgiou, A.G. (2013). DIANA-LncBase: experimentally

verified and computationally predicted microRNA targets on long non-coding RNAs. Nucleic Acids Res. *41*, D239–D245.

37. Wang, P., Ning, S., Zhang, Y., Li, R., Ye, J., Zhao, Z., Zhi, H., Wang, T., Guo, Z., and Li, X. (2015). Identification of lncRNA-associated competing triplets reveals global patterns and prognostic markers for cancer. Nucleic Acids Res. *43*, 3478–3489.

38. Ramanathan, M., Porter, D.F., and Khavari, P.A. (2019). Methods to study RNA-protein interactions. Nat. Methods *16*, 225–234.

39. Statello, L., Guo, C.J., Chen, L.L., and Huarte, M. (2021). Gene regulation by long non-coding RNAs and its biological functions. Nat. Rev. Mol. Cell Biol. *22*, 96–118.

40. Zheng, X., Cho, S., Moon, H., Loh, T.J., Jang, H.N., and Shen, H. (2016). Detecting RNA-protein interaction using end-labeled biotinylated RNA oligonucleotides and Immunoblotting. Methods Mol. Biol. *1421*, 35–44.

41. Rinn, J.L., and Chang, H.Y. (2020). Long noncoding RNAs: molecular modalities to organismal functions. Annu. Rev. Biochem. *89*, 283–308.

42. Zhang, Y., Jiao, L., Sun, L., Li, Y., Gao, Y., Xu, C., Shao, Y., Li, M., Li, C., Lu, Y., et al. (2018). LncRNA ZFAS1 as a SERCA2a inhibitor to cause intracellular Ca(2+) overload and contractile dysfunction in a mouse model of myocardial infarction. Circ. Res. *122*, 1354–1368.

43. Xu, Y., Luo, Y., Liang, C., and Zhang, T. (2020). LncRNA-Mhrt regulates cardiac hypertrophy by modulating the miR-145a-5p/KLF4/myocardin axis. J. Mol. Cell Cardiol. *139*, 47–61.

44. Mariño, G., Pietrocola, F., Eisenberg, T., Kong, Y., Malik, S.A., Andryushkova, A., Schroeder, S., Pendl, T., Harger, A., Niso-Santano, M., et al. (2014). Regulation of autophagy by cytosolic acetyl-coenzyme A. Mol. Cell *53*, 710–725.

45. Ducker, G.S., Chen, L., Morscher, R.J., Ghergurovich, J.M., Esposito, M., Teng, X., Kang, Y., and Rabinowitz, J.D. (2016). Reversal of cytosolic one-carbon flux compensates for loss of the mitochondrial folate pathway. Cell Metab. *23*, 1140–1153.

46. Zhao, Q., Liu, J., Deng, H., Ma, R., Liao, J.Y., Liang, H., Hu, J., Li, J., Guo, Z., Cai, J., et al. (2020). Targeting mitochondria-located circRNA SCAR alleviates NASH via reducing mROS output. Cell *183*, 76–93.e22.

47. Yang, K.C., Yamada, K.A., Patel, A.Y., Topkara, V.K., George, I., Cheema, F.H., Ewald, G.A., Mann, D.L., and Nerbonne, J.M. (2014). Deep RNA sequencing reveals dynamic regulation of myocardial noncoding RNAs in failing human heart and remodeling with mechanical circulatory support. Circulation *129*, 1009–1021.

48. Burzio, V.A., Villota, C., Villegas, J., Landerer, E., Boccardo, E., Villa, L.L., Martínez, R., Lopez, C., Gaete, F., Toro, V., et al. (2009). Expression of a family of noncoding mitochondrial RNAs distinguishes normal from cancer cells. Proc. Natl. Acad. Sci. U S A *106*, 9430–9434.

49. Gao, S., Tian, X., Chang, H., Sun, Y., Wu, Z., Cheng, Z., Dong, P., Zhao, Q., Ruan, J., and Bu, W. (2018). Two novel lncRNAs discovered in human mitochondrial DNA using PacBio full-length transcriptome data. Mitochondrion *38*, 41–47.

50. Zheng, Q., Liu, P., Gao, G., Yuan, J., Wang, P., Huang, J., Xie, L., Lu, X., Di, F., Tong, T., et al. (2019). Mitochondrion-processed TERC regulates senescence without affecting telomerase activities. Protein Cell *10*, 631–648.

51. Cheng, Y., Liu, P., Zheng, Q., Gao, G., Yuan, J., Wang, P., Huang, J., Xie, L., Lu, X., Tong, T., et al. (2018). Mitochondrial trafficking and processing of telomerase RNA TERC. Cell Rep. *24*, 2589–2595.

52. Jourdain, A.A., Koppen, M., Wydro, M., Rodley, C.D., Lightowlers, R.N., Chrzanowska-Lightowlers, Z.M., and Martinou, J.C. (2013). GRSF1 regulates RNA processing in mitochondrial RNA granules. Cell Metab. *17*, 399–410.

53. Noh, J.H., Kim, K.M., Abdelmohsen, K., Yoon, J.H., Panda, A.C., Munk, R., Kim, J., Curtis, J., Moad, C.A., Wohler, C.M., et al. (2016). HuR and GRSF1 modulate the nuclear export and mitochondrial localization of the lncRNA RMRP. Genes Dev. *30*, 1224–1239.

54. Hensen, F., Potter, A., van Esveld, S.L., Tarrés-Solé, A., Chakraborty, A., Solà, M., and Spelbrink, J.N. (2019). Mitochondrial RNA granules are critically dependent on mtDNA replication factors Twinkle and mtSSB. Nucleic Acids Res. *47*, 3680–3698.

55. Dumoulin, B., Ufer, C., Kuhn, H., and Sofi, S. (2021). Expression regulation, protein chemistry and functional biology of the guanine-rich sequence binding factor 1 (GRSF1). J. Mol. Biol. *433*, 166922.

56. Anderson, S., Bankier, A.T., Barrell, B.G., de Bruijn, M.H., Coulson, A.R., Drouin, J., Eperon, I.C., Nierlich, D.P., Roe, B.A., Sanger, F., et al. (1981). Sequence and organization of the human mitochondrial genome. Nature *290*, 457–465.

57. Perales-Clemente, E., Fernández-Silva, P., Acín-Pérez, R., Pérez-Martos, A., and Enríquez, J.A. (2011). Allotopic expression of mitochondrial-encoded genes in mammals: achieved goal, undemonstrated mechanism or impossible task? Nucleic Acids Res. *39*, 225–234.

58. Trajkovski, M., Hausser, J., Soutschek, J., Bhat, B., Akin, A., Zavolan, M., Heim, M.H., and Stoffel, M. (2011). MicroRNAs 103 and 107 regulate insulin sensitivity. Nature *474*, 649–653.

59. Rech, M., Kuhn, A.R., Lumens, J., Carai, P., van Leeuwen, R., Verhesen, W., Verjans, R., Lecomte, J., Liu, Y., Luiken, J., et al. (2019). AntagomiR-103 and -107 treatment affects cardiac function and metabolism. Mol. Ther. Nucleic Acids *14*, 424–437.

60. Jiang, L., Qiao, Y., Wang, Z., Ma, X., Wang, H., and Li, J. (2020). Inhibition of microRNA-103 attenuates inflammation and endoplasmic reticulum stress in atherosclerosis through disrupting the PTEN-mediated MAPK signaling. J. Cell Physiol. *235*, 380–393.

61. Dey, S., DeMazumder, D., Sidor, A., Foster, D.B., and O'Rourke, B. (2018). Mitochondrial ROS drive sudden cardiac death and chronic proteome remodeling in heart failure. Circ. Res. *123*, 356–371.

62. Zhang, Y., Park, J., Han, S.J., Yang, S.Y., Yoon, H.J., Park, I., Woo, H.A., and Lee, S.R. (2020). Redox regulation of tumor suppressor PTEN in cell signaling. Redox Biol. *34*, 101553.

63. Cao, J., Schulte, J., Knight, A., Leslie, N.R., Zagozdzon, A., Bronson, R., Manevich, Y., Beeson, C., and Neumann, C.A. (2009). Prdx1 inhibits tumorigenesis via regulating PTEN/AKT activity. EMBO J. *28*, 1505–1517.

64. Chen, X., Jiang, C., Sun, R., Yang, D., and Liu, Q. (2020). Circular noncoding RNA NR3C1 acts as a miR-382-5p sponge to protect RPE functions via regulating PTEN/AKT/mTOR signaling pathway. Mol. Ther. *28*, 929–945.

65. Nie, X., Fan, J., Li, H., Yin, Z., Zhao, Y., Dai, B., Dong, N., Chen, C., and Wang, D.W. (2018). miR-217 promotes cardiac hypertrophy and dysfunction by targeting PTEN. Mol. Ther. Nucleic Acids *12*, 254–266.

66. Qian, X., Li, X., Shi, Z., Xia, Y., Cai, Q., Xu, D., Tan, L., Du, L., Zheng, Y., Zhao, D., et al. (2019). PTEN suppresses glycolysis by dephosphorylating and inhibiting autophosphorylated PGK1. Mol. Cell *76*, 516–527.e7.

67. Wani, A., Gupta, M., Ahmad, M., Shah, A.M., Ahsan, A.U., Qazi, P.H., Malik, F., Singh, G., Sharma, P.R., Kaddoumi, A., et al. (2019). Alborixin clears amyloid-beta by inducing autophagy through PTEN-mediated inhibition of the AKT pathway. Autophagy *15*, 1810–1828.

68. Chen, C.Y., Chen, J., He, L., and Stiles, B.L. (2018). PTEN: tumor suppressor and metabolic regulator. Front. Endocrinol. *9*, 338.

69. Dou, X., Boyd-Kirkup, J.D., McDermott, J., Zhang, X., Li, F., Rong, B., Zhang, R., Miao, B., Chen, P., Cheng, H., et al. (2019). The strand-biased mitochondrial DNA methylome and its regulation by DNMT3A. Genome Res. *29*, 1622–1634.

70. Wang, G., Chen, H.W., Oktay, Y., Zhang, J., Allen, E.L., Smith, G.M., Fan, K.C., Hong, J.S., French, S.W., McCaffery, J.M., et al. (2010). PNPASE regulates RNA import into mitochondria. Cell *142*, 456–467.

71. Zhang, X., Zuo, X., Yang, B., Li, Z., Xue, Y., Zhou, Y., Huang, J., Zhao, X., Zhou, J., Yan, Y., et al. (2014). MicroRNA directly enhances mitochondrial translation during muscle differentiation. Cell *158*, 607–619.

72. Gao, K., Cheng, M., Zuo, X., Lin, J., Hoogewijs, K., Murphy, M.P., Fu, X.D., and Zhang, X. (2020). Active RNA interference in mitochondria. Cell Res. *31*, 219–228.

73. Jiang, J.G., Ning, Y.G., Chen, C., Ma, D., Liu, Z.J., Yang, S., Zhou, J., Xiao, X., Zhang, X.A., Edin, M.L., et al. (2007). Cytochrome p450 epoxygenase promotes human cancer metastasis. Cancer Res. *67*, 6665–6674.

74. Zhou, Y., Sun, Y., Zhang, J., Cai, J., Dong, N., and Li, F. (2020). Predictors and outcomes of heart transplantation utilizing donors with different brain death mode: a propensity-score matching study from China. Int. J. Cardiol. *322*, 58–64.

75. Li, H., Chen, C., Fan, J., Yin, Z., Ni, L., Cianflone, K., Wang, Y., and Wang, D.W. (2018). Identification of cardiac long non-coding RNA profile in human dilated cardiomyopathy. Cardiovasc. Res. *114*, 747–758.

76. Deng, K.Q., Zhao, G.N., Wang, Z., Fang, J., Jiang, Z., Gong, J., Yan, F.J., Zhu, X.Y., Zhang, P., She, Z.G., et al. (2018). Targeting transmembrane BAX inhibitor motif containing 1 alleviates pathological cardiac hypertrophy. Circulation *137*, 1486–1504.

77. Wu, J., Bu, L., Gong, H., Jiang, G., Li, L., Ma, H., Zhou, N., Lin, L., Chen, Z., Ye, Y., et al. (2010). Effects of heart rate and anesthetic timing on high-resolution echocardiographic assessment under isoflurane anesthesia in mice. J. Ultrasound Med. *29*, 1771–1778.

78. Han, F., Konkalmatt, P., Chen, J., Gildea, J., Felder, R.A., Jose, P.A., and Armando, I. (2015). MiR-217 mediates the protective effects of the dopamine D2 receptor on fibrosis in human renal proximal tubule cells. Hypertension *65*, 1118–1125.

79. Chen, F., Chen, J., Yang, L., Liu, J., Zhang, X., Zhang, Y., Tu, Q., Yin, D., Lin, D., Wong, P.P., et al. (2019). Extracellular vesicle-packaged HIF-1alpha-stabilizing lncRNA from tumour-associated macrophages regulates aerobic glycolysis of breast cancer cells. Nat. Cell Biol. *21*, 498–510.

80. Wang, K., Long, B., Zhou, L.Y., Liu, F., Zhou, Q.Y., Liu, C.Y., Fan, Y.Y., and Li, P.F. (2014). CARL lncRNA inhibits anoxia-induced mitochondrial fission and apoptosis in cardiomyocytes by impairing miR-539-dependent PHB2 downregulation. Nat. Commun. *5*, 3596.

81. Fan, J., Zhang, X., Nie, X., Li, H., Yuan, S., Dai, B., Zhan, J., Wen, Z., Jiang, J., Chen, C., et al. (2019). Nuclear miR-665 aggravates heart failure via suppressing phosphatase and tensin homolog transcription. Sci. China Life Sci. *63*, 724–736.

82. Zhao, Y., Yin, Z., Li, H., Fan, J., Yang, S., Chen, C., and Wang, D.W. (2017). MiR-30c protects diabetic nephropathy by suppressing epithelial-to-mesenchymal transition in db/db mice. Aging Cell *16*, 387–400.

83. Yuan, J.H., Yang, F., Wang, F., Ma, J.Z., Guo, Y.J., Tao, Q.F., Liu, F., Pan, W., Wang, T.T., Zhou, C.C., et al. (2014). A long noncoding RNA activated by TGF-beta promotes the invasion-metastasis cascade in hepatocellular carcinoma. Cancer Cell *25*, 666–681.